

STRUCTURAL DYNAMICS OF FREE MOLECULES AND CONDENSED MATTER.

Part I. THEORY AND EXPERIMENTAL TECHNIQUE

Anatoly A. Ischenko^{1,@}, Yuriy.I. Tarasov¹, Lothar Schäfer²

¹Moscow Technological University (Institute of Fine Chemical Technologies), Moscow, 119571 Russia

²Department of Chemistry and Biochemistry, University of Arkansas, Fayetteville, AR, U.S.A., AR72701

@Corresponding author e-mail: aischenko@yasenevo.ru

To understand the dynamic features of molecular systems with a complex landscape of potential energy surfaces, it is necessary to study them in the associated 4D space-time continuum. The introduction of time in the diffraction methods and the development of coherent principles of the research process opened up new approaches for the study of the dynamics of wave packets, intermediates and transient states of the chemical reactions, short-lived compounds in the gaseous and condensed media. Time-resolved electron diffraction, the new method for the structural dynamic studies of free molecules, clusters and condensed matter, differs from the traditional method of electron diffraction both in the experimental part and in the theoretical approaches used in the interpretation of diffraction data. Here there is particularly pronounced the need of a corresponding theoretical basis for the processing of the electron diffraction data and the results of spectral investigations of the coherent dynamics in the field of intense ultrashort laser radiation. Such unified and integrated approach can be formulated using the adiabatic potential energy surfaces of the ground and excited states of the systems under study. The combination of state-of-the-art optical techniques and electron diffraction methods based on different physical phenomena, but complementing each other, opens up new possibilities of the structural studies at time sequences of ultrashort duration. It provides the required integration of the triad, "structure – dynamics – functions" in chemistry, biology and materials science.

Keywords: structural dynamics, transient structures, transition state for chemical reaction, molecular quantum state tomography, time-resolved electron diffraction, wave packets, coherent nuclear dynamics.

СТРУКТУРНАЯ ДИНАМИКА СВОБОДНЫХ МОЛЕКУЛ И КОНДЕНСИРОВАННОГО СОСТОЯНИЯ ВЕЩЕСТВА. Часть I. ТЕОРИЯ И ЭКСПЕРИМЕНТАЛЬНЫЕ МЕТОДЫ

А.А. Ищенко^{1,@}, Ю.И. Тарасов¹, Л. Шефер²

¹Московский технологический университет (Институт тонких химических технологий), Москва, 119571 Россия

²Факультет химии и биохимии, Университет штата Арканзас, Фэйтвилл, 72701, Арканзас, США

@Автор для переписки, e-mail: aischenko@yasenevo.ru

Для понимания особенностей динамики молекулярных систем со сложным ландшафтом поверхности потенциальной энергии, необходимо исследовать их в четырехмерном пространственно-временном континууме. Введение времени в дифракционные методы и развитие когерентных принципов процесса исследования открывают новые подходы к изучению динамики волновых пакетов, промежуточных и переходных состояний химических реакций, короткоживущих соединений в газовой и конденсированной средах. Дифракция электронов с временным разрешением, новый метод структурных динамических исследований свободных молекул, кластеров и конденсированных сред, отличается от традиционного метода дифракции электронов как по экспериментальному оборудованию, так и те-

оретическими подходами, используемыми при интерпретации дифракционных данных. В методах с временным разрешением особенно выражена необходимость соответствующей теоретической основы для обработки данных дифракции электронов и результатов спектральных исследований когерентной динамики с использованием интенсивного ультракороткого лазерного излучения. Такой единый и комплексный подход можно сформулировать, используя понятие адиабатической поверхности потенциальной энергии основного и возбужденных состояний исследуемых систем. Сочетание самых современных оптических технологий и методов дифракции электронов, основанных на различных физических явлениях, дополняющих друг друга, открывает новые возможности структурных исследований с использованием импульсных последовательностей ультракороткой длительности. Такое сочетание обеспечивает необходимую интеграцию триады «структура – динамика – свойство» в химии, биологии и материаловедении.

Ключевые слова: структурная динамика, промежуточные структуры, переходное состояние химических реакций, томография квантового состояния молекул, электронография с временным разрешением, волновые пакеты, когерентная ядерная динамика.

CONTENTS

Introduction
1. Theory and data analysis in time resolved electron diffraction
1.1. Basic assumptions and approximations
1.2. Time-dependent molecular diffraction intensity
2. Illustration of the diffraction signatures of excited molecules
3. Photodissociation dynamics of spatially aligned molecules by time-resolved electron diffraction
3.1. Coherent nuclear dynamics in aligned molecules: theory elements
3.2. The dynamics of the wave packets
3.3. Modeling the coherent photodissociation dynamics of laser-aligned molecular ensembles
4. Molecular quantum state tomography
4.1. Basic assumptions
4.2. Theoretical approach
4.3. Dual-channel nonadiabatic photodissociation of CS ₂
5. Experimental technique of the time-resolved electron diffraction
5.1. First experiments
5.2. Development of the time-resolved electron diffraction method
Concluding remarks: future outlook
Acknowledgements
References

Introduction

In the beginning of 1980's, the diffraction paradigm was formulated: implementing electron diffraction with time resolution adds a temporal coordinate to the determination of molecular structures [1–4]. Time-resolved electron diffraction (TRED) rested on the concept of flash photolysis originally proposed by Norrish and Porter in 1949 [5]. Advances in the generation of

X-ray pulses have made possible the closely related time-resolved X-ray diffraction (TRXD) [6]. In both methods, short laser pulses create the transient structures and induce chemical dynamics that are subsequently imaged by diffraction at specific time interval.

TRED and TRXD as methods for structural and dynamic studies of fundamental properties differ from traditional diffraction methods in both the experimental implementation and in the theoretical approaches used to interpret the diffraction data [7–9]. The transition to the picosecond and femtosecond temporal scales raises numerous important issues related to the physical essence of the dynamic parameters of the systems studied by analyzing time-dependent scattering intensities. There is a particularly pronounced need of corresponding theoretical basis for the processing of the diffraction data and the results of spectral investigations of the coherent dynamics of non-equilibrium molecular ensembles in the field of intense ultrashort laser radiation. Such a unified and integrated approach can be formulated using the adiabatic potential energy surfaces (APES) of the ground and excited states of the molecular systems under study [10, 11].

To understand the dynamic features of molecular systems within the complex landscapes of APES it is necessary to explore them in the associated 4D space-time continuum. The introduction of time in diffraction methods and the development of foundational principles of their analysis opens up new methodologies to study transient structures of the reaction centers and short-lived intermediate compounds in gaseous and condensed media.

The use of pico- or femtosecond bunches of electrons as probes synchronized with the pulses of the exciting ultrashort laser radiation led to the development of ultrafast electron crystallography and nanocrystallographic techniques [12], of dynamic transmission electron microscopy [13–17] and of molecular quantum state

tomography [18]. One of the promising applications developed by the electron diffraction methods is their use for the characterization and the “visualization” of processes occurring in the photo-excitation of free molecules and biological objects for the analysis of surfaces, thin films, and nanostructures (see the recent review articles [19–29]). The combination of state-of-the-art optical techniques and diffraction methods using different physical phenomena but complementing each other opens up new possibilities for structural research at ultrashort time sequences. It provides the required integration of the triad “Structure-Dynamics-Function” in chemistry, biology, and materials science [15, 16, 23].

1. THEORY AND DATA ANALYSIS IN TIME-RESOLVED ELECTRON DIFFRACTION

1.1. Basic assumptions and approximations

A plane wave electron that is *elastically* scattered by an atom emerges as a spherical wave [30] given by:

$$\Psi(\mathbf{R}, \vartheta) = \frac{\exp(i\mathbf{k}\mathbf{R})}{R} f(\vartheta) \quad (1)$$

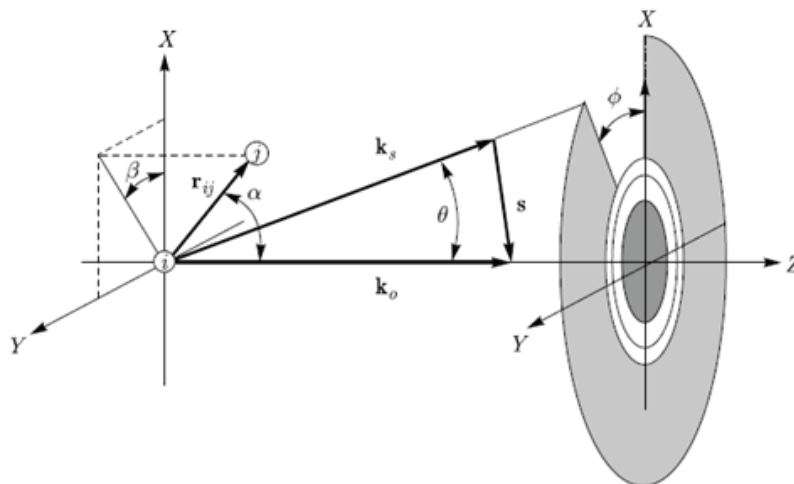


Fig. 1. Definition of scattering coordinates used for the derivation of the intensity equations in electron diffraction. θ is the scattering angle, and ϕ , the azimuthal angle in the detector plane; \mathbf{k}_0 and \mathbf{k}_s are the wave vectors of the incident and scattered electrons, respectively; \mathbf{s} is the momentum transfer vector; \mathbf{r}_{ij} is the internuclear distance vector between the nuclei of atoms i and j , which are positioned at \mathbf{r}_i and \mathbf{r}_j , respectively; α and β give the orientation of the molecular framework with respect to the XYZ laboratory frame.

where \mathbf{k}_0 and \mathbf{k}_s are the wave vectors of the incident and scattered electrons, respectively, and $|\mathbf{k}_0| = |\mathbf{k}_s|$ for elastic scattering. Introducing the momentum transfer vector \mathbf{s} with a magnitude of $|\mathbf{s}| = |\mathbf{k}_0 - \mathbf{k}_s| = \frac{4\pi}{\lambda} \sin(\vartheta/2)$, and invoking the superposition principle, one obtains the amplitude of the electron wave scattered by the molecular system of N atoms as:

where \mathbf{R} is the distance between the scattering center and the detector plane, and the absolute value of the wave vector \mathbf{k} is given by $k = |\mathbf{k}| = \frac{2\pi}{\lambda}$ with λ the wavelength

of the electron. For an isolated atom, the atomic electron scattering amplitude $f(\vartheta)$ determines the amplitude of the electron beam scattered into the angle ϑ (Fig. 1). As the electron traverses the atom, it experiences a phase delay making the scattering factor complex [30]. While for scattering from a single atom this phase shift is inconsequential, scattering from multiple atoms may entail different phase shifts from each individual atom.

The amplitude of the wave scattered by atom i within a molecule is written as [30]:

$$\Psi_i(\mathbf{R}, \vartheta) = \frac{\exp(i\mathbf{k}(\mathbf{R} - \mathbf{r}_i))}{|\mathbf{R} - \mathbf{r}_i|} \exp(ik_0 z_i) f_i(\vartheta), \quad (2)$$

where z_i is the projection of the atomic position vector \mathbf{r}_i onto the Z-axis (Fig. 1), and R is the scattering distance. Since R is a macroscopic parameter (i.e., $r_i \ll R$), eqn. (2) can be expressed as:

$$\Psi_i(\mathbf{R}, \vartheta) = \frac{\exp(i\mathbf{k}\mathbf{R})}{R} \exp(i(\mathbf{k}_0 - \mathbf{k}_s)\mathbf{r}_i) f_i(\vartheta), \quad (3)$$

$$\Psi = \sum_{i=1}^N \Psi_i = \frac{\exp(i\mathbf{k}\mathbf{R})}{R} \sum_{i=1}^N f_i(\mathbf{s}) \exp(i\mathbf{s}\mathbf{r}_i). \quad (4)$$

The intensity of the scattered electrons can be expressed in terms of the electron current density \mathbf{j} [11]:

$$\mathbf{j}(\mathbf{s}) = \frac{eh}{4i\pi m_e} (\Psi * \nabla \Psi - \Psi \nabla \Psi^*), \quad (5)$$

where e and m_e are the electron charge and mass, ∇ the gradient operator, and Ψ^* the complex conjugate wave function Ψ , eqn. 4.

Using Eqns. (4) and (5) one obtains for the intensity:

$$I(s) = I_o(\mathbf{j}_{sc}/\mathbf{j}_o) = I_o \operatorname{Re} \frac{1}{2ik_o} \sum_{i=1}^N \Psi_i^* \nabla \Psi_i - \Psi_i \Psi_i^* = \frac{I_o}{R^2} \operatorname{Re} \left(\sum_{i=1}^N f_i(s) \exp(i\mathbf{s}\mathbf{r}_i) \sum_{j=1}^N f_j^*(s) \exp(-i\mathbf{s}\mathbf{r}_j) \right) = \frac{I_o}{R^2} \left(\sum_{i=1}^N |f_i(s)|^2 + \operatorname{Re} \sum_{i \neq j=1}^N f_i(s) f_j^*(s) \exp(i\mathbf{s}(\mathbf{r}_i - \mathbf{r}_j)) \right) \quad (6)$$

In equation 6, I_o is the intensity of the incident electron beam, $\mathbf{j}_o = \frac{eh\mathbf{k}_o}{2\pi m_e}$ and \mathbf{j}_{sc} are the current densities for the incident and the scattered electrons, respectively. Re denotes the real part of the function. Higher order terms corresponding to multiple scattering are neglected for the current purpose.

Equation (6) is often written as $I(s) = I_a(s) + I_{mol}(s)$ where the first term is ascribed to the incoherent “atomic scattering”, because it does not depend on the internuclear distances. The second term, which does depend on the internuclear distances, is ascribed to the coherent “molecular scattering”. For each pair of atoms (i, j) separated by the instantaneous internuclear distance, $\mathbf{r}_{ij} = \mathbf{r}_i - \mathbf{r}_j$ eqn. (6) yields the molecular intensity function:

$$I_{mol}(s) = \frac{I_o}{R^2} \operatorname{Re} \sum_{i \neq j=1}^N |f_i(s)| |f_j(s)| \exp(i\Delta\eta_{ij}(s)) \exp(i\mathbf{s}\mathbf{r}_{ij}) \quad (7)$$

$$I_{mol}(s, t) = \left\langle \left\langle I_{mol}(s) \right\rangle_{vib} \right\rangle_{sp} = \frac{I_o}{R^2} \sum_{i \neq j=1}^N |f_i(s)| |f_j(s)| \operatorname{Re} \left(\exp(i\Delta\eta_{ij}(s)) \left\langle \left\langle \exp(i\mathbf{s}\mathbf{r}_{ij}) \right\rangle_{vib} \right\rangle_{sp} \right) = \frac{I_o}{R^2} \sum_{i \neq j=1}^N |f_i(s)| |f_j(s)| \operatorname{Re} \left(\exp(i\Delta\eta_{ij}(s)) \int_0^\infty P_{vib}(r_{ij}, t) \int_0^{\pi} \int_0^{2\pi} P_{sp}(\alpha_{ij}, \beta_{ij}, t) \exp(i\mathbf{s}\mathbf{r}_{ij}) \sin(\alpha_{ij}) d\beta_{ij} d\alpha_{ij} dr_{ij} \right) \quad (8a)$$

In eqn. 8a, $\langle \dots \rangle$ denotes the vibrational and spatial (orientational) averaging over the scattering ensemble, $P_{vib}(r_{ij}, t)$ and $P_{sp}(r_{ij}, \alpha_{ij}, \beta_{ij}, t)$ are the vibrational and spatial p.d.f., respectively, and α_{ij} and β_{ij} are the angles of the spherical polar coordinate system (Fig. 1) that define the

$$I_{mol}(s, t) = \frac{I_o}{R^2} \sum_{i \neq j=1}^N |f_i(s)| |f_j(s)| \cos(\Delta\eta_{ij}(s)) \int P_{vib}(r_{ij}, t) \left[\sin(sr_{ij}) / sr_{ij} \right] dr_{ij} \quad (8b)$$

The time-dependent p.d.f., $P_{sp}(\alpha_{ij}, \beta_{ij}, t)$ and $P_{vib}(r_{ij}, t)$ in eqn. 8a, determine the molecular intensity function, $I_{mol}(s, t)$ at each point in time, t . The former describes the evolution of the spatial distribution in the system under investigation. The vibrational p.d.f. describes the evolution of structure in the ensemble of

where $\Delta\eta_{ij}(s)$ is the difference in the phase shifts incurred by the electrons while scattering from atoms i and j , respectively [31].

Inherent in eqn. 7 is an approximation known as the Independent Atom Model (IAM), which assumes that the electronic wave function of each atom in a molecule is just that of the isolated atom [30]. This implies that the effects of chemical bonding on the electron density distribution of the atoms are ignored. Within the IAM approximation, the molecular surrounding of an atom does not affect its scattering, so that tabulated atomic scattering factors can be used for each atom in a molecule.

Assuming single scattering processes for fast electrons (> 10 keV) with short (attosecond) coherence time, the electrons encounter molecules that are essentially “frozen” in their rotational and vibrational states. Thus, the latter can be accounted for by using probability density functions (p.d.f.) that characterize the ensemble under investigation.

1.2. Time-dependent molecular diffraction intensity

If the molecular systems investigated are not at equilibrium, as is the case in studies of laser-excited molecules, a time-dependent p.d.f. must be used to describe the structural evolution of the system. In addition, rotational and vibrational motions can be separated adiabatically, since the latter involves much faster processes.

In TRED the time-dependent molecular intensities can then be represented by averaging eqn. 7 with the p.d.f. that represents the spatial and vibrational distributions of the scattering ensemble [32, 33]:

orientation of the internuclear distance vector \mathbf{r}_{ij} in the scattering coordinate frame.

For spatially isotropic, randomly oriented molecules, $P_{sp}(\alpha_{ij}, \beta_{ij}) = 1/4\pi$, and eqn. 8a simplifies to the following expression for the time-dependent molecular intensity function:

laser-excited species. In what follows, we concentrate on internuclear dynamics that evolves on a time-scale much shorter than the orientational effects, such as the rotational recurrence [11]. Therefore, only the time-independent spatial p.d.f., $P_{sp}(\alpha_{ij}, \beta_{ij})$, will be considered in the current analysis. For spatially

anisotropic ensembles the theory will be presented in Section 3. For the particular case of a molecular

ensemble at thermal equilibrium, eqn. 8b can be written in the form first derived by Debye [34]:

$$I_{mol}(s) \propto \text{Re} \sum_{i \neq j=1}^N f_i^*(s) f_j(s) \langle \sin(sr_{ij})/sr_{ij} \rangle_{vib-rot} = \sum_{i \neq j=1}^N |f_i(s)| |f_j(s)| \cos(\eta_i(s) - \eta_j(s)) \int [\sin(sr_{ij})/sr_{ij}] dF_T(r_{ij}) \quad (9)$$

where $dF_T(r_{ij})$ is the probability distribution function at the vibrational temperature T , and $dF_T(r_{ij}) = P_T(r_{ij}) dr_{ij}$.

As in the time-independent case, the method of averaging in eqns. 8a,b may be defined freely, so long as certain conditions of convergence and normalization are fulfilled. The modified molecular intensity function $sM(s,t)$ can be calculated as:

$$sM(s,t) = sI_{mol}(s,t)/I_{at}(s), \quad (10)$$

where $I_{at}(s)$ is the atomic background [31] considered here to be time-independent.

We now consider more generally the intensities of electrons scattered by a molecular ensemble after excitation by a short laser pulse. Let us assume that

the laser field produces a wave packet [35] of highly vibrationally excited states that propagates on the potential energy surface of the excited electronic state of the molecule. The time-dependent function $\Psi(r,t)$ of the wave packet can be expanded in terms of the orthonormal basis functions $\phi_n(r)$ in the following way (see, for example, [36]):

$$\Psi(r,t) = \sum_{n=0}^{\infty} C_n \phi_n \exp(-2\pi i E_n t/h) \quad (11)$$

where n is the quantum number identifying the state with energy E_n , C_n is the amplitude, and the $\phi_n(r)$ are a complete set of arbitrary analytic functions.

The modified molecular intensity for randomly oriented species can then be represented by [37]:

$$sM(s,t) = g(s) \int \Psi^*(r,t) \Psi(r,t) [\sin(sr)/r] dr = g(s) \sum_{n,m=0}^{\infty} C_n^* C_m \exp(-2\pi i \Delta E_{nm} t/h) \int \phi_m^*(r) \phi_n(r) [\sin(sr)/r] dr \quad (12)$$

where $\Delta E_{nm} = E_m - E_n$, and $g(s)$ is the reduced atomic scattering factors [31].

Therefore, the radial distribution function obtained from a time resolved electron diffraction (TRED) experiment, i.e., the Fourier transform $F(r,t)$ of the modified molecular intensity $sM(s,t)$, also depends explicitly on both the internuclear distances and the time. Thus, it contains direct information on the time-evolution of the molecular structure through:

$$F(r,t) = \sqrt{\frac{2}{\pi}} \int sM(s,t) \exp(isr) ds \quad (13)$$

Applying the general form of the molecular intensities, eqn. (8b), to the one-dimensional case, it is possible to write:

$$sM(s,t) = g(s) \int P(r,t) [\sin(sr)/r] dr \quad (14)$$

where $P(r,t) = \Psi^*(r,t) \Psi(r,t)$ and, consequently:

$$F(r,t) \propto P(r,t)/r \quad (15)$$

Thus, eqns. 12–15 show that in TRED, the modified molecular intensities of scattered electrons depend explicitly on both the time-evolution of internuclear distances and the energy distribution. Averaging the molecular intensity function $sM(s,t)$ over an electron pulse profile function $I_0(s; t_d)$ yields the TRED

diffraction intensities $sM(s; t_d)$ parametrically dependent on the delay time t_d between the pump laser pulse and the electron probe pulse of duration τ :

$$\langle sM(s; t_d) \rangle_{\tau} = \int_t^{t+\tau} I_0(t'; t_d) sM(s, t') dt' \quad (16)$$

In this way data refinement involves minimization of the functional:

$$\sum_{i=1}^m \left[\langle s_i M(s_i; t_d) \rangle_{\tau, \text{exp}} - R \langle s_i M(s_i; t_d) \rangle_{\tau, \text{theo}} \right]^2, \quad (17)$$

where m is the number of data points, and R the index of resolution.

The solution of the inverse diffraction problem is a characteristically ill-posed problem [38], and it is described for TRED data refinement in the monograph [7] (Chapter 4, Section 3). For now we will illustrate the effect of molecular excitation on electron diffraction patterns using some specific examples.

2. ILLUSTRATION OF THE DIFFRACTION SIGNATURES OF EXCITED MOLECULES

The separation of conventional, gas phase electron diffraction signatures into an incoherent ‘atomic’ scattering term and a coherent ‘molecular’ scattering term, $I_{\text{total}}(s) = I_{\text{atomic}}(s) + I_{\text{mol}}(s)$, is a mathematical construct that aids the extraction of the oscillations

due to the molecular structure from the overall electron diffraction signal that decays rapidly with increasing momentum transfer. But it would, of course, not be correct to understand the scattering from a molecule as comprised of distinct and additive atomic and molecular intensity terms. Rather, the diffraction signal represents the Fourier transform of the molecular structure, as defined by the complete molecular probability density function including its electronic, vibrational and rotational parts. The small modulation depth of observed electron diffraction signals of gas phase samples stems from the orientational averaging over isotropic molecular ensembles and from the Gaussian-like distributions of internuclear separations in most thermal samples.

It is then interesting and instructive to consider the diffraction patterns that would result from molecules excited to specific, well-defined quantum states. Such patterns, for CS_2 molecules elevated to certain vibrational states, have been calculated by Ryu, Weber and Stratt [39]. Fig. 2 shows the vibrational probability density distribution in the laboratory frame, when the molecule is excited to a state with nine quanta of bending vibration. The motions of the carbon atom and the sulfur atoms are manifested in the oscillations of the wave function. Since the mass of sulfur is much larger than that of carbon, the displacement of the latter greatly exceeds those of the former: the carbon atom essentially swings between the almost-stationary sulfur atoms.

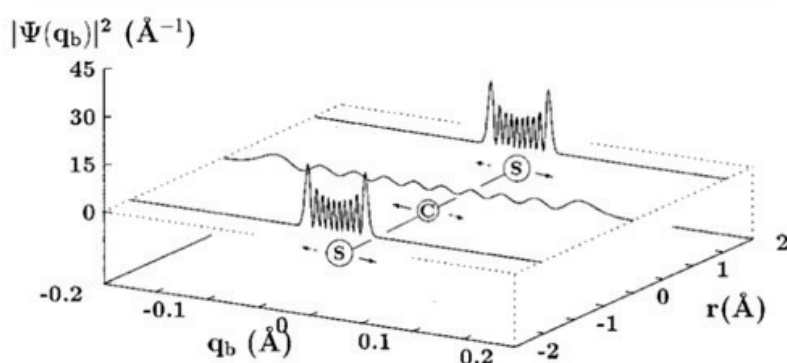


Fig. 2. The probability density distribution $|\Psi(q_b)|^2$ of the vibrational motions when 9 quanta of vibrational energy are in the bending mode (q_b) of the CS_2 molecule (zero vibrational angular momentum).

For this illustration, the amplitudes of vibrations in the other three normal modes are not shown. From ref. [39].

Vibrational excitation of a molecule to a state such as the one shown in Fig. 2 imparts additional modulations in the diffraction pattern, which Ryu [et al.] [39] have calculated.

For molecules that are clamped at specific orientations with respect to the incoming electron beam and the outgoing scattered beam, Fig. 3 shows the resulting diffraction patterns.

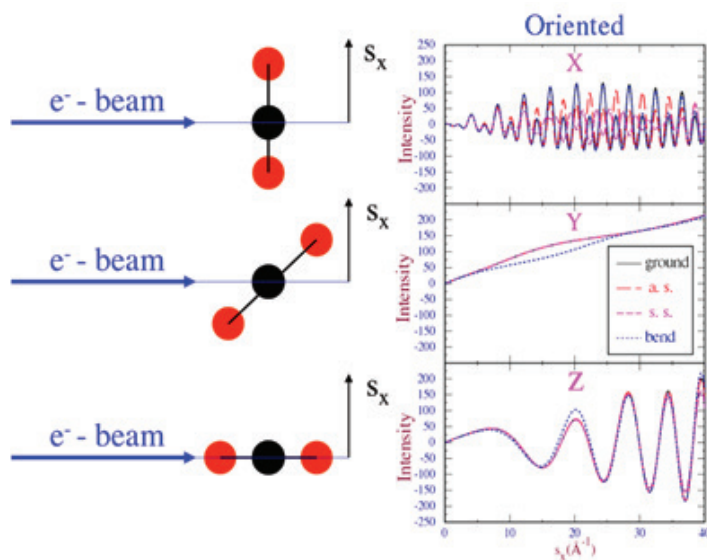


Fig. 3. For CS_2 molecules clamped at specific orientations, different diffraction patterns result from different vibrational excitations. Plotted at the right are the molecular components of the diffraction patterns, for the molecule in the vibrational ground state, and for molecules excited by four quanta of symmetric stretch (s.s.), antisymmetric stretch (a.s.) and the bending vibration. From ref. [39].

Note in Fig. 3 that when the CS_2 molecules are aligned perpendicular to the direction of observation, X, and the electron beam, Z, the molecular part of the diffraction signature is almost featureless: the wavelets originating at each of the atoms are (almost) always in phase (middle frame, black curve, which is underneath the pink one). When the molecule is excited to either the symmetric or the antisymmetric stretch vibration, there is no change: all those traces are on top of each other. However, when the bend vibration is excited (blue dotted trace), the molecular probability density function picks up an out-of-plane oscillatory structure that gives rise to a slight modulation in the diffraction pattern.

For scattering of electrons into the X-direction from X-aligned CS_2 molecules (top frame), the electron diffraction signal is more sensitive to the molecular structure, as seen by the rapidly oscillating (black) trace

of the ground state molecule. Excitation of either the symmetric stretch or the antisymmetric stretch vibrations causes additional oscillations that are easily observed in the diffraction trace. In this geometry, the excitation of out-of-plane motions in the bend vibration does not, however, lead to additional oscillations, so that the diffraction traces of so excited molecules closely resemble that of the ground state molecule. For molecules aligned with the incoming electron beam (bottom), it is again the out-of-plane vibration that is captured in the diffraction trace.

These concepts can be readily extended to the diffraction signatures of larger vibrating polyatomic molecules. In the papers [40–42] it has been calculated the patterns expected when the cyclic, 6-atomic aromatic ring molecule s-tetrazine ($\text{C}_3\text{H}_3\text{N}_3$) is excited to specific vibrations in its electronically excited state S_1 . Fig. 4 illustrates the richly structured nature of the diffraction

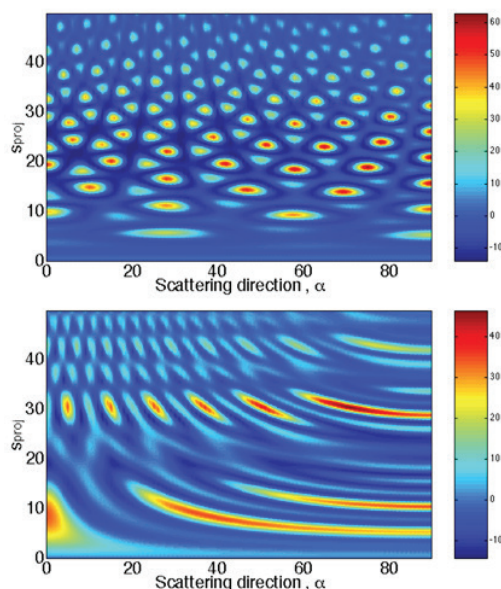


Fig. 4. Diffraction signal expected for s-tetrazine clamped in specific geometries with respect to the incoming and the outgoing electron beams. The images show the diffraction signals for molecules in their ground vibrational states, for molecules with the aromatic plane perpendicular to the electron beam (top) and with the electron beam parallel to the aromatic plane (bottom). Plotted are the diffraction signals as a function of momentum transfer, s_{proj} and the angle of rotation about the electron beam axis, α . From ref. [40].

signal that would be obtained when the molecules were clamped at specific orientations with respect to the incoming and the outgoing beams.

Even in the polyatomic s-tetrazine molecule, vibrational excitation leads to additional structure in the diffraction patterns, because the vibrational p.d.f modulates the molecular structure. Importantly, this modulation still manifests itself when isotropically distributed molecules in the gas phase are investigated: excitation with a linearly polarized laser beam induces a sufficient anisotropy to make the observation of the vibrational modes possible. Fig. 5 illustrates this on a variety of vibrational motions in the excited S_1 electronic state of s-tetrazine. Noteworthy is that again, the out-of-

plane bending vibrations (mode 16a) have qualitatively different diffraction signatures than the in-plane stretch vibrations (modes 1 and 6a).

3. PHOTODISSOCIATION DYNAMICS OF SPATIALLY ALIGNED MOLECULES BY TIME-RESOLVED ELECTRON DIFFRACTION

Because of the chaotic orientation of molecules in the gas phase, unlike X-ray diffraction by a crystal, the electron diffraction technique in the absence of additional information (e.g., about equilibrium configuration symmetry of the study system, equivalence of certain

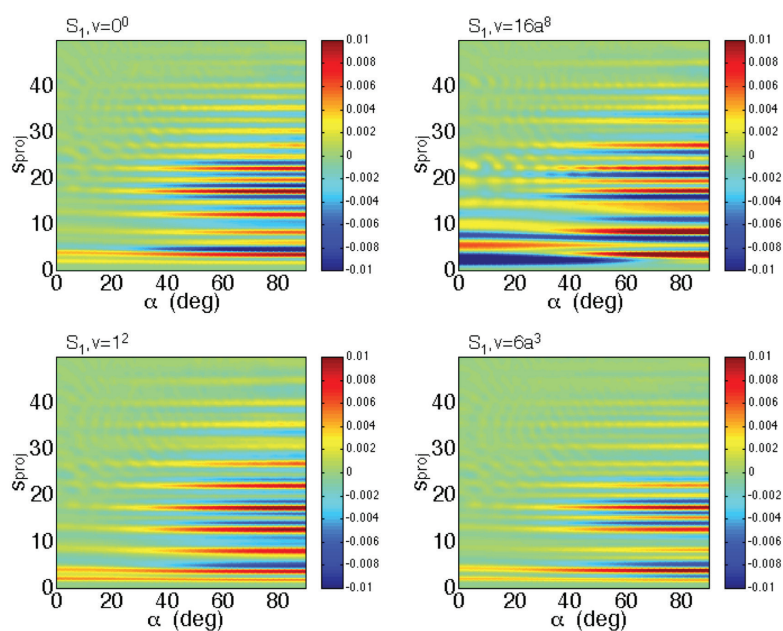


Fig. 5. Diffraction patterns (difference between excited state patterns and the ground state patterns) of s-tetrazine, where a polarized laser excites the molecules of an isotropic sample to specific vibronic states. The abscissa gives the rotation about the electron beam axis, with the laser polarization at $\alpha = 0^\circ$, and the ordinate is the projection of the s-vector onto the detector. From ref. [42].

chemical bonds, character of vibrational energy distribution) permits determining only a one-dimensional molecular structure or a set of internuclear distances. It restricts applications of the electron diffraction method for studying the structure and dynamics of complex polyatomic molecules. The solution of a structure-related problem even in the case of relatively small molecules implies the involvement of results obtained by other experimental methods, such as vibrational spectroscopy and/or quantum-chemical computation [43–48].

X-ray crystallography is believed to be the most adequate tool for the elucidation of the structure of complex polyatomic molecules. However, this method can be applied only for the study of crystalline objects. Moreover, the local environment of a molecule distorts its structure and makes it difficult to study the nuclear dynamics.

A new approach to structural research based on isolated molecule irradiation by a large number of photons contained in a single X-ray laser pulse was proposed in ref. [48]. The use of ultrashort laser pulses enabled the researchers to obtain diffraction patterns before the study system was destroyed. Diffraction patterns for micro- and nanometer objects were taken with femtosecond pulses of soft X-ray radiation [49–52]. However, this method is currently employed only in studies of fairly large objects, such as nano-sized particles.

The schematic experimental layout for TRED study of aligned molecules is presented in Fig. 6. A linearly polarized laser pulse (ϵ) excites molecules in the gas phase, and the sample is diagnosed by an electron pulse generated with a given delay time. The laser and electron beams intersect at 90° . The electron pulse scattered from the sample is a bunch

of electrons; its longitudinal extent is $v\Delta t$, where v is the electron velocity, and Δt is the pulse length.

Each point on the detector (Fig. 6) is characterized by the scattering angle θ and azimuth angle ϕ , which corresponds to the wave vector \mathbf{k} and the vector of momentum transfer \mathbf{s} . Radial distance between the registration point and the center of the unscattered electron beam denoted as s' is given as a function of s , \mathbf{k} , and L – the distance from the scattering point to the center of the diffraction pattern on the detector. *Insert:* the schematic representation of the time series of the dipole transitions of molecules in the scattering volume. At $t = 0$ the laser pulse, which has a vertical polarization, crosses the volume creating a certain population of excited states consisting of molecules having dipole transitions primarily oriented in the vertical direction. Rotation with different angular velocities, both excited and unexcited molecules, leads to a loss of the original order. On a significantly longer time intervals that order can be restored after the rotational revival of the wave packet. From ref. [53]

The pulse (electron bunch) leaving the scattering volume makes up the central core of unscattered electrons surrounded by the expanding cloud of scattered electrons of varying intensity shown in the figure in the form of rings. The electron diffraction pattern is taken far from the scattering center in a relatively small region of scattering angles on a flat detector, the center of which coincides with the incident beam axis. Each point on the detector is characterized by scattering angle θ and azimuthal angle ϕ corresponding to the wave vector

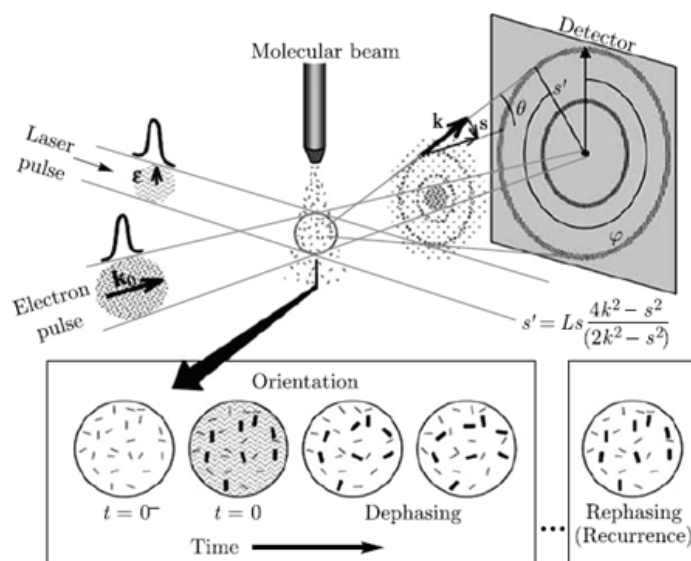


Fig. 6. Ultrafast electron diffraction experimental setup for studying anisotropic ensembles of laser-excited molecules.

The linearly polarized laser pulse (ϵ) excites the molecules in the gas phase, and the sample is diagnosed using an electron pulse with a certain time delay. Laser and electron beams intersect at an angle of 90° . Electron pulse scattered by the sample has longitudinal dimensions equal to $v\Delta t$, where v is the speed of the electrons, and Δt is the pulse duration.

The electron bunch leaving the scattering region is represented by a central core of the unscattered electrons surrounded by an expanding cloud of scattered electrons. Electron diffraction pattern is recorded at a distance from the scattering center in a relatively small range of scattering angles on the flat detector. From ref. [53].

\mathbf{k} and the momentum variation vector \mathbf{s} . The radial distance between the registration point and the center of the unscattered beam denoted by \mathbf{s}' is presented in the figure as the expression through quantities s and k ; the camera distance between the scattering point and the center of the diffraction pattern on the detector is denoted by L (Fig. 6).

An alternative approach takes advantage of the TRED method as applied to anisotropic ensembles ('oriented' molecules whose dipole transitions are oriented in the direction of polarization of the laser radiation) in the gas phase. The anisotropic environment of laser-excited molecules can be formed, for example, under the effect of fs pulses of polarized laser radiation. It was theoretically predicted in refs. [11, 32, 39–41, 53, 54] that the electron diffraction pattern from 'oriented' molecules in the gas phase furnishes an opportunity of determining not only internuclear distances, but also valence angles.

The theory was first confirmed experimentally in refs. [55–57] for adiabatically oriented CS_2 molecules using the TRED method with a resolution of 10 ns. To elucidate the structure of organic molecules, such as low-molecular weight proteins scarcely amenable to crystallization, the authors of ref. [58] used a jet of liquid gel droplets and a continuous electron beam producing a diffraction pattern. Organic molecules, e.g., small proteins, in a droplet or inside a glassy ice shell can be spatially oriented under the effect of polarized radiation of a powerful continuous wave laser. Iterative methods for solving the phase problem have been proposed.

3.1. Coherent nuclear dynamics in aligned molecules: theory elements

The interaction of ultrashort pulses of polarized laser radiation with an isotropic medium of randomly oriented molecules leads to photoexcitation of molecules whose dipole moments are oriented in the direction of polarization of the laser radiation.

Thus, the spatial anisotropy of coherently excited molecules is created generating different types of spatial order of the ensemble. The electron scattering theory for spatially oriented ensembles of molecules require substantial modification of the electron diffraction theory for randomly oriented molecules in the gas phase [11, 32, 39–41, 53, 54]. Assuming single scattering processes for fast electrons (>10 keV) with short (attosecond) coherence time, the electrons encounter molecules that are essentially "frozen" in their rotational and vibrational states. Thus, the latter can be accounted for by using probability density functions (p.d.f.) that characterize the ensemble under investigation. TRED experimental geometry for laser-aligned molecules is shown on Fig. 7.

If the molecular systems investigated are not at equilibrium, as is the case in studies of laser-excited molecules, a time-dependent p.d.f. must be used to describe the structural evolution of the system. In addition, rotational and vibrational motions can be separated adiabatically, since the latter involves much faster processes.

The equation for the time-dependent molecular scattering intensity can be written as follows (please, see, e.g. ref. [32]):

$$I_{mol}(s,t) = \left\langle \left\langle I_{mol}(s) \right\rangle_{vib} \right\rangle_{sp} = \frac{I_0}{R^2} \sum_{i \neq j=1}^N |f_i(s)| |f_j(s)| \operatorname{Re} \left\{ \exp(i\Delta\eta_{ij}(s)) \left\langle \exp(isr_{ij}) \right\rangle_{vib} \right\rangle_{sp} = \frac{I_0}{R^2} \sum_{i \neq j=1}^N |f_i(s)| |f_j(s)| \cos(\Delta\eta_{ij}(s)) \int_0^\infty P_{vib}(r_{ij},t) \left[\int_0^{\pi/2} \int_0^{2\pi} P_{sp}(\alpha_{ij},\beta_{ij},t) \exp(isr_{ij}) \sin(\alpha_{ij}) d\beta_{ij} d\alpha_{ij} \right] dr_{ij} \quad (18)$$

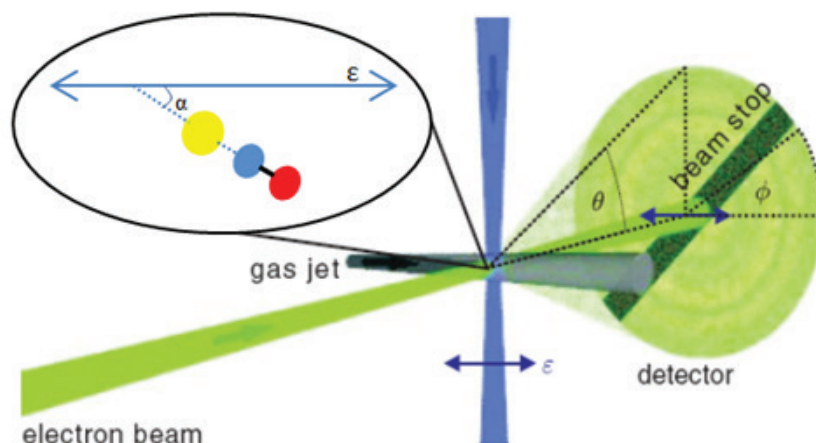


Fig. 7. TRED experimental geometry for laser-aligned molecules: the electron beam, laser beam, and gas jet are mutually orthogonal. The polarization of the laser beam is orthogonal to the direction of propagation of the electron beam. θ is the scattering angle, and ϕ is the azimuthal detector angle with respect to the laser polarization. ϵ laser polarization (blue arrow), ICN molecule (schematic); α : angle between the C-I bond (dissociation axis) and laser polarization. The constituent atoms are color-coded, with yellow for iodine, light-blue for carbon, and red for nitrogen. From ref. [59] with minor revision.

In eqn. 18, $\langle \dots \rangle$ correspond to vibrational and spatial (orientational) averaging over the scattering ensemble. $P_{vib}(r_{ij},t)$ and $P_{sp}(\alpha_{ij},\beta_{ij},t)$ – vibrational and orientational probability density functions (p.d.f.), respectively; α_{ij} and β_{ij} are angles in the spherical polar coordinate system (Fig. 1), which defines the orientation of the internuclear distance vector \mathbf{r}_{ij} .

Time-dependent functions $P_{sp}(\alpha_{ij},\beta_{ij},t)$ and $P_{vib}(r_{ij},t)$ in eqn. 18 determine the molecular scattering intensity at time t . The first function determines the evolution of the spatial distribution. Vibrational probability density function describes the structural dynamics in the ensemble of laser-excited particles. Orientational probability density function for an ensemble of laser-excited molecules is described in several publications [60–62]. A systematic study was carried out by Zare [61]. In this study there were obtained equations in classical and quantum mechanical approximations. For spatial anisotropy produced via plane-polarized laser beam, both approximations yield similar results.

While eqn. 18 is general enough for description of polyatomic molecules, we first consider the case of linear polyatomic molecules. For electron scattering on oriented linear molecules we need to consider two main cases: scattering from molecules oriented parallel to the primary electron beam, which will be called the *parallel scattering*, and scattering from molecules oriented

perpendicular to the incident electron beam, which we call *perpendicular scattering*. In the first case, $P_{sp}(\alpha,\beta;t)$ depends only on angle α (Fig. 1), since the polarization of the laser beam is collinear to axis Z. Laser radiation at the initial time $t = 0$ separates the excited and unexcited molecules ensembles. In this case, the p.d.f. can be written as [60, 61]:

$$\|P_{sp}^{ex}(\alpha) = (3/4\pi)\cos^2\alpha \quad (19)$$

$$\|P_{sp}^{unex}(\alpha) = (3/8\pi)\sin^2\alpha \quad (20)$$

where $\|P_{sp}^{ex}$ and $\|P_{sp}^{unex}$ refer to the excited and unexcited ensembles, respectively.

For perpendicular scattering, the polarization vector of the laser beam is perpendicular to the Z axis, and the p.d.f. is dependent on the angle α and the angle β :

$$\perp P_{sp}^{ex}(\alpha,\beta) = (3/4\pi) \sin^2\alpha \cos^2\beta \quad (21)$$

$$\perp P_{sp}^{unex}(\alpha,\beta) = (3/8\pi) [1 - \sin^2\alpha \cos^2\beta] \quad (22)$$

The scalar product $(\mathbf{s}\mathbf{r}_{ij})$ in eqn. 18 can be written in terms of trigonometric functions of angles α and β , which determine the orientation of the vector \mathbf{r}_{ij} in coordinates of scattering angles θ and ϕ , which describe electron scattering:

$$(\mathbf{sr}_{ij}) = [-\cos\phi\cos(\theta/2)\sin\alpha\cos\beta - \sin\phi\cos(\theta/2)\sin\alpha\sin\beta + \sin(\theta/2)\cos\alpha]sr_{ij} \quad (23)$$

Using the eqn. 18 and p.d.f. (eqns. 19–22), after integration by α and β [63, 64] we obtain the intensities for parallel molecular scattering of electrons:

$$\|I_{\text{mol}}^{\text{ex}}(s,t) = (I_0/R^2)\sum_{i \neq j=1}^N |f_i(s)| |f_j(s)| \cos(\Delta\eta_{ij}(s)) \int P_{\text{vib}}(r_{ij},t) \{[\sin(sr_{ij})/sr_{ij}] \cdot [(1/s^2r_{ij}^2)(1-3s^2/4k_0^2)+s^2/4k_0^2] - [\cos(sr_{ij})/s^2r_{ij}^2](1-3s^2/4k_0^2)\} dr_{ij} \quad (24)$$

$$\|I_{\text{mol}}^{\text{unex}}(s,t) = (I_0/R^2)\sum_{i \neq j=1}^N |f_i(s)| |f_j(s)| \cos(\Delta\eta_{ij}(s)) \int P_{\text{vib}}(r_{ij},t) \{[\sin(sr_{ij})/sr_{ij}] \cdot (1-s^2/4k_0^2) - [\cos(sr_{ij}) - \sin(sr_{ij})/sr_{ij}](1/s^2r_{ij}^2)(1-3s^2/4k_0^2)\} dr_{ij} \quad (25)$$

As can be seen from eqns. 24, 25, the dependence on the wavelength of electrons ($k_0 = 2\pi/\lambda$) is weak for electrons with energies greater than 10 keV in the whole range of typical values of s . Moreover, just as in the case of isotropically oriented molecules, scattering intensity

is axially symmetric and depends only on the scattering angle θ .

In contrast to this result, the intensity of perpendicular molecular scattering is not axially symmetric and explicitly depends on the azimuthal angle ϕ :

$$\perp I_{\text{mol}}^{\text{ex}}(s,\phi,t) = (I_0/R^2)\sum_{i \neq j=1}^N |f_i(s)| |f_j(s)| \cos(\Delta\eta_{ij}(s)) \cdot \int P_{\text{vib}}(r_{ij},t) \{[\sin(sr_{ij})/(sr_{ij}) - \cos(sr_{ij})](1/sr_{ij})^2 - (1-s^2/4k_0^2)[(3/s^3r_{ij}^3 - 1/sr_{ij}) \cdot \sin(sr_{ij}) - (3/s^2r_{ij}^2)\cos(sr_{ij})]\cos^2\phi\} dr_{ij} \quad (26)$$

$$\perp I_{\text{mol}}^{\text{unex}}(s,\phi,t) = (I_0/R^2)\sum_{i \neq j=1}^N |f_i(s)| |f_j(s)| \cos(\Delta\eta_{ij}(s)) \cdot \int P_{\text{vib}}(r_{ij},t) \{[\sin(sr_{ij})/(sr_{ij})][1 - (1-s^2/4k_0^2)\cos^2\phi] + [\cos(sr_{ij}) - \sin(sr_{ij})/(sr_{ij})] \cdot (1/sr_{ij})^2 [1 - (1-s^2/4k_0^2)3\cos^2\phi]\} dr_{ij} \quad (27)$$

For derivation of those equations, each p.d.f. (eqns. 19–22) was normalized. Therefore, $I_{\text{mol}}(s,t)$ represented by eqns. 24–27 are also normalized [32]. In the ensemble of excited and unexcited particles there must be introduced corresponding relative weights of these states. Equations (24–27) require explicit expressions for $P_{\text{vib}}(r_{ij}, t)$, which can be represented, for example, on the basis of a stochastic approach to the analysis of electron diffraction data [11].

For accounting for quantum effects in the diffraction intensity it is required to define time-dependent p.d.f., $P(r,t) = |\Psi(r,t)|^2$ by solving corresponding time-dependent Schrödinger equation. Various approaches for solving this problem were suggested [65–67]. In an article of [32] it is suggested utilizing FGH (Fourier Grid Hamiltonian) method [67–69].

3.2. The dynamics of the wave packets

The experimental exploration of isolated molecular systems with high temporal resolution involves the creation and detection of wave packets. A wave packet can be described as a coherent superposition of certain eigenstates $\langle N|$. By the definition, the exact (not in the approximation of Born-Oppenheimer) eigenstates are the solutions of the time-independent Schrödinger equation and are stationary. Therefore, the dependence on time appears only because of the superposition of the different

states and arises from the quantum-mechanical phases $\exp(-2\pi i E_N t/h)$ that are associated with each eigenstate. Conceptually, a "pump-probe" experiment has three stages: (1) the preparation of the molecule in the excited state (the pump); (2) the dynamical evolution of the wave packet; (3) the probe of the transient superposition of states. A typical femtosecond "pump-probe" experiment is illustrated in Fig. 8 [70]. As a result of the two-photon transition created by the pump and the probe pulses, the final state $|\Psi_f\rangle$ arises at the end of the sequence of two laser pulses. Since the two-photon transition is coherent, we should sum up the transition amplitudes and then square the sum to get the final probability. As it will be discussed later, the signal contains the interference between all components of the degenerate two-photon transitions.

If the temporal delay between the two laser pulses is changed, the phase relations between the amplitudes of the two-photon transitions also change, which in turn leads to a change in the interference in the final state of the wave packet.

During the interaction of the pump laser pulse, the amplitudes and the initial phases of the set of eigenstates corresponding to the first excited state are determined by the amplitude and the phase of this laser pulse and the amplitudes of the dipole moments of the transition between the ground and the first excited state. At the end

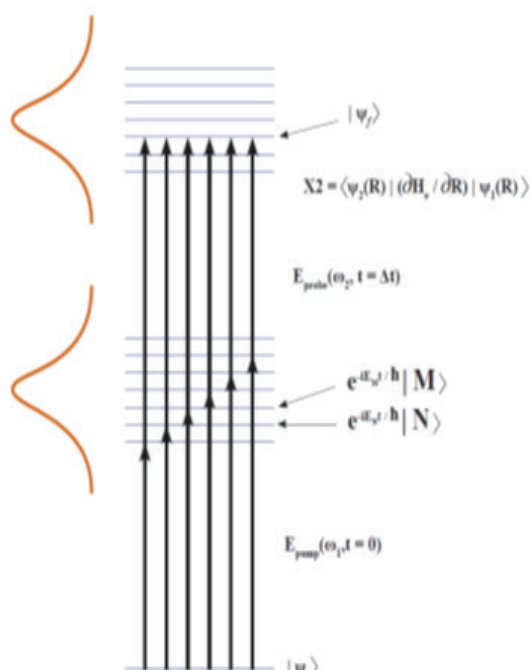


Fig. 8. Creation, evolution and detection of a wave packet.

The pump laser pulse E_{pump} (black) creates a coherent superposition of the molecular eigenstates from the ground state $|\Psi_i\rangle$ at time $t = 0$.

The set of eigenstates $|N\rangle$ in this superposition (a wave packet) has different phase factors, which results in non-stationary behavior, i.e., the evolution of the wave packet. At time $t = \Delta t$, the wave package is projected by the probe pulse E_{probe} (gray) to a set of the final states $|\Psi_f\rangle$, which act as a "template" for the dynamics. Here the time-dependent probability to be in the given final state $|\Psi_f\rangle$ is modulated by the interference between the amplitudes of all degenerate coherent two-photon transitions, which leads to the final state. From ref. [70] with minor revision.

of the pump pulse the wave packet $\Psi(t)$ undergoes a free evolution in accordance with the equation:

$$|\Psi(t)\rangle = \sum_N A_N \exp(-2\pi i E_N t/h) |N\rangle \quad (28)$$

The complex coefficients A_N in eqn. 28 contain both the amplitudes and the initial phases of the exact eigenstates of the molecule $|N\rangle$, each with energy E_N , which are prepared by the action of the pump laser pulse. The probe laser pulse interacts with the wave packet at the end of the pump pulse projecting the wave packet on the chosen final state $|\Psi_f\rangle$ at some temporal delay $t = \Delta t$. This final state is the "template", onto which the wave packet dynamics is projected. The temporal dependence of the differential signal for the projection onto a single final state can be written as

$$S_f(t) = |\langle \Psi_f | E_{\text{probe}}(\omega) d | \Psi(t) \rangle|^2 = |\sum_N B_N \exp(-2\pi i E_N t/h)|^2, \quad (29)$$

where the complex coefficients B_N contain both the amplitudes of the wave packet A_N and the (complex) elements of the matrix of the transition dipole moment under the influence of the pump pulse and link each state with the final state in the superposition $|N\rangle$:

$$B_N = A_N \langle \Psi_f | E_{\text{probe}}(\omega) d | N \rangle \quad (30)$$

Thus, the eq. (29) can be rewritten as:

$$S_f(t) = 2 \sum_N \sum_{M < N} |B_N| |B_M| \cos[2\pi(E_N - E_M)t/h + \Phi_{NM}], \quad (31)$$

where the phase factor Φ_{NM} contains the initial phase differences of the eigenstates of the molecule and the phase differences of the matrix elements of the dipole moment transition to the excited state by the action of the pump pulse, connecting the states $|N\rangle$ and $|M\rangle$ to the final state. *This differential signal of the final state, $S_f(t)$, contains the most detailed information:* it arises from the coherent sum over all amplitudes of two-photon transitions within the bandwidth of the laser pump and probe pulses and contains the interference components between all degenerate two-photon transitions [70]. It is clearly seen that the signal as a function of temporal delay $t = \Delta t$ contains modulations at the frequencies of $2\pi(E_N - E_M)/h$ corresponding to the set of energy differences in the superposition. This equation gives the relationship between the dynamics of the wave packet and the observed pump-probe signal. It is the interference between the individual two-photon transitions through the different excited eigenstates, but terminating in the same final state. Therefore, the Fourier transform of the signal in this temporal interval contains the frequencies that yield the energy level differences of the excited state. A similar expression is observed in the intensity of the electron scattering in the diffraction experiments.

3.3. Modeling the coherent photodissociation dynamics of laser-aligned molecular ensembles

To illustrate the basic effects arising in the scattering time-dependent intensities and their corresponding Fourier transforms (the radial distribution functions of the inter-atomic distances), we will focus on the linear triatomic molecules (A-B-C), in which the action of a laser pulse breaks the bond A-B. In many cases, the potential function for such systems can be expressed as [71]:

$$V(R, r) = V_0 \exp[-(R - \gamma r)/\rho], \quad (32)$$

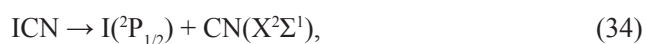
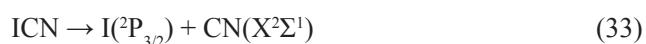
where R is the distance between the nucleus A and the center of mass of the fragment B-C in the molecule A-B-C; $r = r_0(BC) - r_c(BC)$; $\gamma = m_c/(m_B + m_C)$; $r_0(BC)$ and $r_c(BC)$ – internuclear distance in the ground vibrational state and the equilibrium internuclear distance of the

fragment B-C, respectively; ρ is a so-called range parameter [71, 72]. The reactions and APES of this kind are well known for a number of systems [71–73]. At the first stage of the analysis, the manifestation of nuclear dynamics in the scattering of ultrashort pulses of fast electrons by systems dissociating in accordance with adiabatic potential functions was demonstrated.

The ground state of the ICN molecule is approximated by the Morse function with the parameters: $a_M = 190 \text{ pm}^{-1}$; R_e (the equilibrium distance from the iodine atom to the center of mass of the molecule) = 261.7 pm, $D_e = 26340 \text{ cm}^{-1}$. The dissociative state is selected from several that are possible, and it obeys eqn. (12), with the parameters $V_0 = 242720 \text{ cm}^{-1}$, $R_0 = 262.2 \text{ pm}$ and $\rho = 80 \text{ pm}$, as given in refs. [73, 74].

The photodissociation of ICN has been studied extensively both by experimental and theoretical methods, including femtosecond transient state spectroscopy (please see ref. [75] and references therein).

The dissociation of ICN ($210 < \lambda < 350 \text{ nm}$) proceeds via two channels [75,76]:



producing the CN radicals predominantly in the ground electronic state $\text{X}^2\Sigma^1$, and the iodine atoms in the ${}^2\text{P}_{3/2}$ and ${}^2\text{P}_{1/2}$ states. The vibrational distribution of the CN fragment of the ICN molecule was measured [74] and at 266 nm it was found that vibrational population ratios, $n(v=1)/n(v=0) = 0.012$; $n(v=2)/n(v=0) = 6 \times 10^{-4}$; $n(v=3)/n(v=0) = 1 \times 10^{-4}$.

In the 266 nm photolysis, the experiment [77] determined rotational distribution of the radicals can be presented as a sum of three B_0 main distributions centered at the rotational temperatures $T_1 = 37(3) \text{ K}$, T_2

= 489(12) K and $T_3 = 6134(250) \text{ K}$, with approximately equal in grated fractional populations.

Rotational excitation of the CN fragments requires an additional term in the potential function, eqn. (32), and can be approximated in diffraction intensities by including the centrifugal distortion δr of the $r(\text{CN})$ internuclear distance in a relatively long time range. However, considering time scale of the dissociation, the evolution of the angular momentum can be neglected.

In a series of studies (please see, e.g., ref. [75] and references cited therein) it was shown that, at the wavelength of 306 nm, the dissociation channel leading to the iodine excited state $\text{I}({}^2\text{P}_{1/2})$ is effectively closed. Thus, based on the experimental studies described in ref. [75], in our model calculations the dissociation of the ICN was assumed to proceed via a stretching reaction coordinate, and the parameters of ref. [75] for the dissociative potential leading to $\text{I}({}^2\text{P}_{3/2})$ were used (eqn. 33). The molecular electron diffraction intensities, $sM(s)$, for the molecules in their ground state were calculated with the parameters of refs. [32] and [74] using standard computational procedures [78].

One approach that can be used to describe the dynamics of the excited molecules is an approximation of the wave packet [79–82]. The wave packet carries the information on the relative positions and nuclear momenta, as well as their components at different APES, corresponding to different electron states [80, 81]. For the wave function with minimal uncertainty Gaussian function can be used as the basis for the creation of the wave functions of the system, as it was proposed in refs. [81–83] (please, see also ref. [80]). Considering the classical trajectory in the phase space, where the Hamiltonian in the vicinity of the moving point $\{p(t); R(t)\}$ can be expressed in terms of the degrees of $(p - \langle p(t) \rangle)$ and $(R - \langle R(t) \rangle)$ up to the second order, the wave function is defined as follows [81]:

$$\Psi(r,t) = \exp\left\{ (2\pi i/h) [\alpha(t)(R - \langle R(t) \rangle)^2 + \langle p(t) \rangle (R - \langle R(t) \rangle) + \gamma(t)] \right\}, \quad (35)$$

where $\alpha(t)$ gives the spreading of the wave packet, $\gamma(t)$ is its complex phase, and $\langle \dots \rangle$ is the expected value. Using the time-dependent Schrödinger equation we can obtain the differential equations for the position and the momentum:

$$\partial \langle R(t) \rangle / \partial t = \langle p(t) \rangle / m \text{ and } \partial \langle p(t) \rangle / \partial t = - \langle \partial V(R) / \partial R \rangle, \quad (36)$$

where $V(R)$ is the potential in the Born-Oppenheimer approximation. The eqns (36) describe the trajectory of the wave packet. For large time delays after excitation of the investigated molecules and the use of longer probing electron pulses, it is necessary to take into account the increase in the width (spread) of the wave

packet manifested in the diffraction pattern. In this case, the probability density of interatomic distances in an ensemble of dissociating molecules can be represented as follows:

$$P(R, t) = [2\pi\sigma^2(t)]^{-1/2} \exp\{-[R - R(t)]^2 / 2\sigma^2(t)\}, \quad (37)$$

where $\sigma(t=0)$ is the dispersion of the wave packet at the initial time of the laser excitation, and $R(t)$ is the classical trajectory of the center of gravity of the wave packet. Consequently, the dispersion of the propagating wave packet can be expressed as a linear function of time during its free motion:

$$\sigma(t) = \sigma(0) [1 + h^2 t^2 / 16\pi^2 m^2 \sigma^4(0)]^{1/2}. \quad (38)$$

If the pulse laser pump has a form of δ -function at $t = 0$, the temporal dependence of the molecular intensity will be:

$$sM(s, t) = g(s) \int (\sin(sR)/R) P(R, t) dR. \quad (39)$$

When the form of the probing electron pulse is approximated by the Gaussian function with the central point $t = t_0$ and corresponding duration of τ , the averaged molecular intensities can be written as:

$$\langle sM(s, t) \rangle_\tau = (2\pi\tau^2)^{-1/2} \int \exp[-(t-t_0)^2/2\tau^2] sM(s, t) dt \quad (40)$$

Using the above theory, time-dependent molecular scattering intensities and the corresponding radial distributions of internuclear distances in the ICN photodissociation processes were calculated [84], Fig. 9 (please, see Reference [83] for comparison of results).

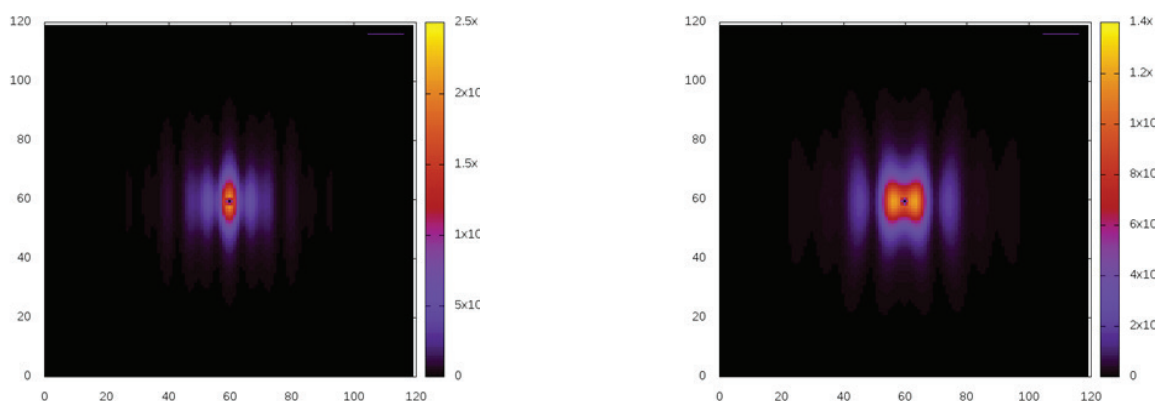


Fig. 9. Difference in molecular scattering intensities $\Delta sM(s, \phi)$ of isotropic and anisotropic vibrationally excited nonequilibrium molecular ensembles of ICN molecules for angles $\phi = 0$ (upper part), and 90° (lower part). Linear polarization of laser radiation is along the axis X (perpendicular scattering). From ref. [84].

Comparison of the diffraction intensities for parallel and perpendicular scattering (eqns. (24) and (26)) shows differences (Fig. 9) in the angular dependence of the molecular intensities. The intensity pattern of the latter is no longer axially symmetric, the essential features can still be recorded with a linear detector system, such as a CCD camera. This is because all angular effects at the detector can be measured by rotating the plane of polarization of the laser light. The vibrational p.d.f. is rather flexible for use in studies of different types of vibrational distributions in laser-excited molecules [11, 32]. It can be used in analyses of TRED

data by refining the parameters that define $P_{\text{vib}}(r, t)$, directly from the experimental data. However, it cannot be applied to dissociative processes, because the cumulant expansion does not converge in such cases (please see monograph [7] of Ischenko, Girichev and Tarasov, Part IV).

Correlations between wave packet dynamics and the modes of laser excitation are important for spectroscopic investigations, but not for electron scattering. Thus, they were not taken into account in the current modeling calculations. Some representative results for ICN obtained in this way are given in Figs. 10 and 11.

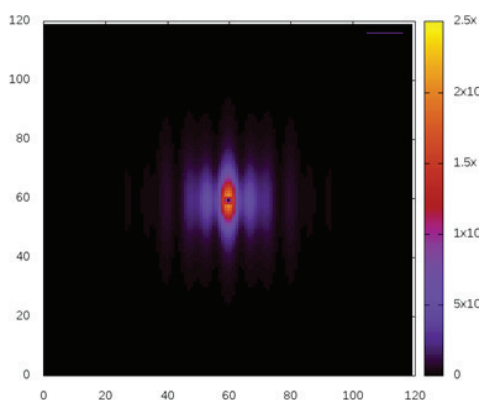


Fig. 10. Diffraction intensity pattern for aligned laser photodissociating ICN molecules. Probe time $t = 200$ fs and the probe pulse duration $\tau = 25$ fs. From ref. [84].

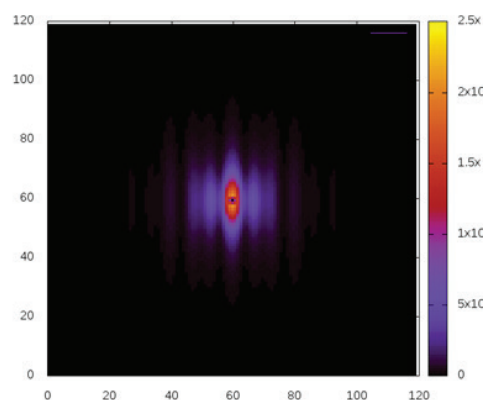


Fig. 11. Radial distribution functions for aligned laser photodissociating ICN molecules. Probe time $t = 200$ fs and the probe pulse duration $\tau = 25$ fs. From ref. [84].

The speed of propagation of the ICN wave packet is faster in the current calculations than in those reported previously [11]. This is because the speed of propagation of the center of gravity of the wave packet in the calculations of ref. [11] depends on the asymptotic group velocity $v = (2E/m)^{1/2}$, which in turn depends on the available energy E . The present calculations refer to slightly higher available energy values.

The good agreement between the two sets of results – those based on quantum dynamical calculations and those based on the Gaussian wave packet approximation [11, 32] – is an important finding, because the latter represent a more straightforward and convenient method for analysing TRED data in terms of a limited number of adjustable parameters which can be refined more readily from the experimental data.

4. MOLECULAR QUANTUM STATE TOMOGRAPHY

4.1. Basic assumptions

In accordance with the basic principles of quantum mechanics, the state of a single molecule cannot be determined experimentally [85]. However, for an ensemble of identical systems it is possible to determine their density matrix. Knowing the status of the system means that we have the most information about all physically measurable quantities [86]. The density matrix and the probability density function in the phase space – the Wigner function [87–90] – have a one-to-one correspondence [91], which describes the maximum of the available statistical information. Therefore, when the term molecular quantum state is used, the quantum state of the ensemble of molecules is assumed.

In 1933, it was demonstrated [92] (see also [85]) that a pure quantum state $|\Psi\rangle$ can be recovered from the time-dependent probability density function $P(\mathbf{r},t) = |\Psi(\mathbf{r},t)|^2$ and its derivative $\partial P(\mathbf{r},t)/\partial t$. Pure quantum state can also be recovered by measuring $P(\mathbf{r},t)$ at time t and its time sequence (evolution) through a fairly short interval Δt , that is, as shown in $P(\mathbf{r},t + N\Delta t) = |\Psi(\mathbf{r},t + N\Delta t)|^2$ ($N = 0, 1, 2, \dots$) [93].

Scattering intensities in TRED have a *direct correlation with the time-dependent probability density function of internuclear distances* $P(\mathbf{r},t)$. In TRED pulsed electron source is utilized for probing the ensemble of ensembles of particles in a certain time sequence. Synchronized electron and laser pulses provide a stroboscopic picture of the evolving process. Thus, an additional variable is introduced into the measurements, which is time. It becomes possible to study the coherent dynamics of the nuclei in the laser-excited systems, the transition state of the chemical reaction and the dynamics of molecular wave packets [11, 33, 83, 94–96]. TRED method can be utilized for probing dynamics of wave packets – coherent superposition of quantum states

created by short optical pulses with controlled phase [97–102]. Consequently, it becomes possible to directly observe the coherent nuclear dynamics of excited molecules [11, 33, 37, 83] as a single act of the elastic electron scattering occurs on the attosecond time scale [10, 11].

The time-dependent intensities of molecular scattering of electrons $M(\mathbf{s},t)$, obtained using TRED with coherent excitation of the molecular system provide the possibility of determining the fundamental elements of the density matrix and the tomographic reconstruction of molecular quantum state of the system.

4.2. Theoretical approach

In TRED (UED) a function of the intensity of the molecular scattering of $M(\mathbf{s},t)$ is determined:

$$M(\mathbf{s},t) = (I_0/R^2) g(\mathbf{s}) \operatorname{Re} \int P(\mathbf{r},t) \exp(i\mathbf{s}\mathbf{r}) d\mathbf{r} \quad (41)$$

In eqn. 41, I_0 is the profile of the incident electron pulse [10, 11], R is the distance from the scattering point to the detector, $g(\mathbf{s})$ is the scattering function [30], and $(\mathbf{s}\mathbf{r})$ is the scalar product of the scattering vector \mathbf{s} and the vector of interatomic distances \mathbf{r} . The integration in eqn. 41 and subsequent equations is carried out in an infinite domain.

In classical mechanics, there is no equation describing the evolution of the probability density function $P(\mathbf{r},t)$ and $P(\mathbf{p},t)$; only the joint probability density function, $W_{cl}(\mathbf{p},\mathbf{r},t)$, can be expressed using Liouville equation [88]. Therefore, there are no corresponding quantum equations for $P(\mathbf{r},t)$, as well as $P(\mathbf{p},t)$. However, the known Wigner-Liouville equation [89, 90] can be used to describe the evolution of the Wigner function – $W(\mathbf{r},\mathbf{p},t)$. For derivation of the equation describing the time-dependent function of the molecular component of the scattering intensity $M(\mathbf{s},t)$ via Wigner function, consider some boundary properties of $W(\mathbf{r},\mathbf{p},t)$:

$$\int W(\mathbf{p},\mathbf{r},t) d\mathbf{p} = P(\mathbf{r},t) \quad (42)$$

$$\int W(\mathbf{p},\mathbf{r},t) d\mathbf{r} = P(\mathbf{p},t) \quad (43)$$

The function $M(\mathbf{s},t)$, eqn. 41, can be written as [103]:

$$M(\mathbf{s},t) = (I_0/R^2) g(\mathbf{s}) \operatorname{Re} \int d\mathbf{p} \int W(\mathbf{r},\mathbf{p},t) \exp(i\mathbf{s}\mathbf{r}) d\mathbf{r} \quad (44)$$

Equation 44 is the most general representation of the intensity of the molecular scattering in TRED, expressed in terms of the Wigner function. *In this representation of $M(\mathbf{s},t)$ can be interpreted as a filtered projection of the Wigner function, where the scattering operator $\exp(i\mathbf{s}\mathbf{r})$ is a filter, modified by scattering functions $g(\mathbf{s})$.* For many problems Wigner function $W(\mathbf{r},\mathbf{p},t)$ can be derived

in analytical form (see, for example, a review articles [89, 90]) or by solving Wigner-Liouville equations numerically with the corresponding potential function of the molecule.

In equations 41 and 42, $P(r,t) = |Y(r,t)|^2$, and in general, it is assumed that $Y(r,t)$ can describe a mixed quantum state. The wave function $\Psi(r,t)$ can be represented as an expansion in orthonormal basis

functions $\psi_n(r)$ as follows:

$$\Psi(r,t) = \sum_n C_n \psi_n(r) \exp(-i\omega_n t) \quad (45)$$

where n is the quantum number of states with energy E_n , ω_n is the frequency of oscillations, and C_n is the probability amplitude. Then, the equation 44 can be written as:

$$M(s,t) = (I_0/R^2) g(s) \sum_{m,n} \rho_{mn} \exp[i(\omega_m - \omega_n)t] \langle \psi_m(r) | \exp(isr) | \psi_n(r) \rangle \quad (46)$$

where ρ_{mn} are the elements of the density matrix.

Equation 46 shows that the intensity of the molecular scattering explicitly depends on the quantum state of the

molecular system. Accordingly, the probability density function $P(r,t)$, which can be obtained using TRED data as the Fourier transform of equation 41:

$$P(r,t) = (2/\pi)^{1/2} (R^2/I_0) \int M(s,t) [g(s)]^{-1} \exp(-isr) ds = \\ (2/\pi)^{1/2} \sum_{m,n} \rho_{mn} \exp[i(\omega_m - \omega_n)t] \int \langle \psi_m(r) | \exp(isr) | \psi_n(r) \rangle \exp(-isr) ds, \quad (47)$$

depends on the internuclear distance r and time t , explicitly contains all the information about the quantum state of the system, and represents a projection (or "shadow": [104]) of the Wigner function.

The interference term in the intensity of molecular scattering of electrons (equation 46 and its Fourier image, equation 47) gives the principal possibility for determining the density matrix ρ and performing tomographic reconstruction of molecular quantum state of the system [11, 105, 106]. Thus, using the temporal sequence of the TRED measurements of the scattering intensity $M(s,t)$ and the Fourier transform (equation 47), we obtain the required information for the tomographic reconstruction of the Wigner function $W(r, p)$. For this purpose, we can use the Radon transform [104, 107–109]:

$$W(r,p) = -\mathbf{P}/(2\pi^2\hbar) \iint P(x,\Theta) (r \cos\Theta + p \sin\Theta - x)^{-2} dx d\Theta \quad (48)$$

where \mathbf{P} is Cauchy principal value, and $\Theta = \omega t$ is angle of rotation in the phase space [107] corresponding to the time of motion t on the potential energy surface of the molecule.

In Equation (48), the integration must be performed in the range $0 \leq \Theta \leq 2\pi$. This means that in order to determine the total quantum state of the system, measurements of the scattering intensity $M(s,t)$ must be performed by the TRED method for a "tomographically complete" set [110], in which the wave packet completed the total recovery period corresponding to the T_{rev} time [11]. Consequently, the measurements of $M(s,t)$ must be performed on a time interval $0 \leq t \leq T_{rev} = 2\pi/\omega$, which corresponds to the complete rotation cycle of the Wigner function. When

using the full data set for tomographic reconstruction of coherent state the wave packet at $t = 0$, the Wigner function, $W(r,p,0)$ can be recovered using the inverse Radon transform using equation 48. Similarly, by taking measurements of the scattering intensity in the time interval of $0 + N\tau_d \leq t \leq T_{rev} + N\tau_d$, where N is integer, and τ_d is delay of the laser and electron pulse, the Wigner function can be restored for time, $N\tau_d$. Therefore, TRED provides the capability for recovery of quantum state of the molecules in the ensemble.

Another method for recovery of molecular quantum state is determining the elements of the density matrix, ρ_{mn} , which have a one-to-one correspondence [91, 111] with the Wigner function:

$$W(r,p) = (1/\pi\hbar) \int \exp(2ipx/\hbar) \langle r-x | \rho | r+x \rangle dx \quad (49)$$

where ρ is the density matrix [86]:

$$\rho = \sum_{n,m} \rho_{nm} |\psi_n(r)\rangle \langle \psi_m(r)|. \quad (50)$$

In the case when the measurements are performed for incomplete cycle determined by the time interval $0 + N\tau_d \leq t \leq T_{rev} + N\tau_d$, only by the diagonal elements of the density matrix can be determined, $\rho_n = \rho_{nn}$. Determination can be performed using a probability density function $\langle P(r,t) \rangle_\tau$ averaged over the time interval $\tau \gg \sup(|\omega_m - \omega_n|^{-1})$, $m \neq n$, as was demonstrated in [104, 108, 110, 112–114]:

$$\rho_{nn} = \int \langle P(r,t) \rangle_\tau \{ \partial[\psi_n(r) \phi_n(r)] / \partial r \} dr, \quad (51)$$

where $\psi_n(r)$ is a regular normalizable solution of time-independent Schrödinger equation, and $\varphi_n(r)$ is the second linearly independent innormalizable solution [115–119].

The results of such a procedure for tomographic reconstruction of molecular quantum state of N_2 and CS are described in [11, 120] and are presented in Fig. 12 and in Table.



CS_2 molecule in the excited state is quasilinear, but has the equilibrium internuclear distances different from those in ground electronic state. Predissociation of CS_2 takes place in ~ 1 ps.

CS_2 in a supersonic molecular beam with laser irradiation at a wavelength of 193 nm demonstrates [121, 122] that the

4.3. Dual-channel nonadiabatic photodissociation of CS_2

Photochemistry of CS_2 molecule was thoroughly investigated in the 180–210 nm range [121,122]. Upon photoexcitation with 193 nm photons photodissociation takes place via dual-channel mechanism:

initial distribution of vibrational energy in the CS molecule, the photodissociation product, is inverted for both dissociation channels (1D_2 and 3P_2). The initial distribution of vibrational energy in CS is described as a bimodal [121] or broad [122] distribution with a low population level for $n = 0$ and $n \geq 10$, as shown in Table 1.

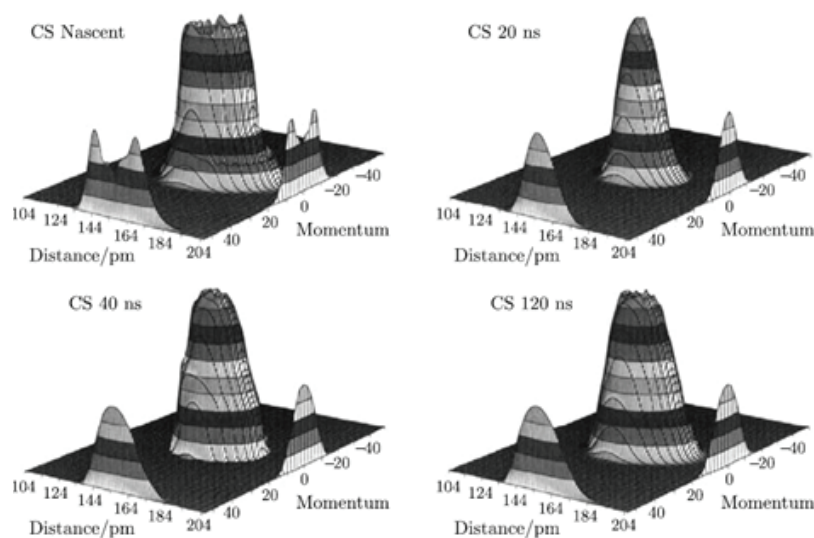


Fig. 12. Wigner function for CS molecule. For the initial distribution (~ 1 ps) Wigner function is determined using the full density matrix. Wigner functions for the delay τ_d 20, 40 and 120 ns were obtained by tomographic reconstruction using the procedure described above. From ref. [18].

Table 1. The diagonal elements of the density matrix for N_2 and CS molecules [18]. Illustration of the accuracy reduction of the molecular quantum state by TRED

n / ρ_{nn}	0	1	2	3	4	5	6	7	8	9	10	11	12	13	14
N_2 (exp) ^a	0.9938	0.0011	0.0102	-0.000	0.001	0.005	-0.009	0.012	-0.011	0.009	-0.005	--	--	--	--
N_2 (theor) ^b	0.9935	0.0064	0.0000	0.000	0.000	0.000	0.000	0.000	0.000	0.000	0.000	0.000	0.000	0.000	0.000
CS (nasc) ^c	0.000	0.049	0.098	0.156	0.101	0.077	0.061	0.070	0.073	0.077	0.077	0.073	0.067	0.021	0.000
CS (nasc) ^d	0.000	0.074	0.148	0.236	0.153	0.116	0.083	0.042	0.042	0.032	0.023	0.023	0.028	--	--
CS (20 ns) ^e	0.349	0.260	0.172	0.099	0.053	0.025	0.013	0.000	-0.001	-0.003	0.001	--	--	--	--
CS (40 ns) ^e	0.204	0.190	0.160	0.129	0.097	0.075	0.058	0.033	0.005	-0.015	-0.015	--	--	--	--
CS (120 ns) ^e	0.173	0.165	0.147	0.124	0.100	0.080	0.058	0.040	0.029	0.021	0.013	--	--	--	--

^aThe values were obtained by electron diffraction at $T = 673$ K. The accuracy of detection is 0.01.

^bCalculated values for the Boltzmann distribution at $T = 673$ K.

^cThe values obtained for the initial distribution (~ 1 ps) in the CS molecule [122].

^dValues derived from the nascent ensemble of CS reported in [18].

^eThe data obtained from TRED measurements with time delay $\tau_d = 20, 40$ and 120 ns after photodissociation of CS_2 molecule followed by photoexcitation with 193 nm photons [18, 121].

The experimental results show that in the first 20 ns the system rapidly evolves to equilibrium, which corresponds to the collisionless intermolecular transfer of vibrational energy (probably due to dipole-dipole interactions). During this time, a bimodal distribution in momentum space, and the space of interatomic distances, becomes monomodal, more narrow distribution (Fig. 12). In the interval from τ_d from 20 to 40 ns collisional energy transfer begins to dominate the collisionless process. Thus, changes between 20 and 40 ns demonstrate the conversion of electronic energy into vibrational via collisions with $S(^1D_j)$ atoms and molecules $CS(X^1\Sigma_g^+)$. Between 40 and 120 ns, saturation of this process takes place.

As is seen from Table 1, there is a significant decrease in the populations of the first three vibrational levels of CS between 20 and 120 ns. The most likely explanation of this effect is the transfer of vibrational energy into rotational and translational degrees of freedom of the CS molecule. This hypothesis is supported by an increase in rotational temperature of CS in the process of collisions, from $T_{rot} = 4200 \pm 300$ K at 20 ns to 5000 ± 600 K at 120 ns [18, 101, 121]. Bimodality of the probability density functions in momentum space, $P(p,t)$, and in the space of interatomic distances, $P(r,t)$ (please see Fig. 12) reflects the fact that photo-dissociation of CS_2 at pump photon wavelength of 193 nm occurs via two channels with formation of atoms $S(^3P_j)$ and $S(^1D_j)$.

To date, a significant progress in generation of ultrashort electron pulses and measuring their characteristics has been achieved (see, for example,

[14, 124–129] and references therein). A technique which allows for generation of sub 100 fs laser pulses was proposed [124, 130]. Approaches for generation of electron pulse with duration of about 1 fs were also suggested [131]. For femtosecond electron pulses, the interval for time averaging τ which is dependent on the probability density function $P(r,t)$ which satisfies: $\tau < \sup(|\omega - \omega_n|^{-1})$, $m \neq n$. For example, for I_2 molecule, the potential energy surfaces of which are well studied [132], with excitation using 520 nm femtosecond laser pulse to the $B(O_u^+)$ state τ is ~ 1 ps [103, 104]. Thus, with femtosecond time resolution TRED opens the possibility for studying the coherent nuclear dynamics and tomographic recovery of wavepacket dynamics.

5. Experimental technique of the time-resolved electron diffraction

Formulation of the main principles of the time-resolved electron diffraction method and pioneering experiments showing the possibility of introducing a time coordinate in electron diffraction date back in the USSR to the late 1970s and early 1980s [1, 2, 4, 133]. Flash photolysis method proposed by Norrish and Porter [5] in 1949 was used as a prototype. By that time, it had been understood that spectral methods provide only indirect information on the structural dynamics of the molecule's nuclear subsystem (see refs. [11, 37] for a detailed discussion of this point).

The concept of the time-resolved electron diffraction method is illustrated in Fig. 13.

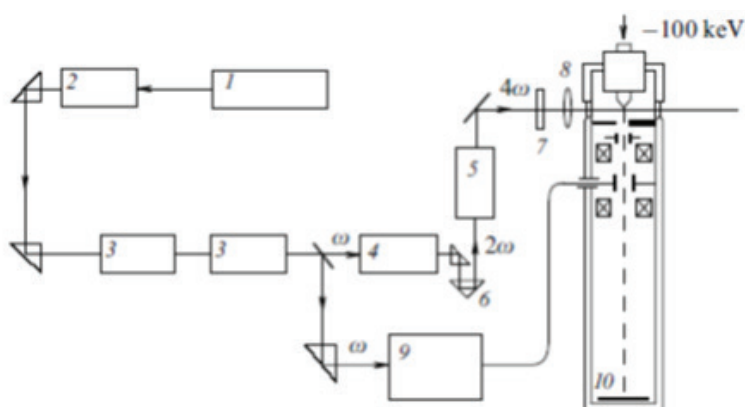


Fig. 13. Schematic of the first TRED setup for the study of coherent nuclear dynamics of the free molecules and condensed matter: 1 – Nd:YAG laser; 2 – single-pulse generator; 3 – amplifiers; 4 – second harmonic generator (SHG); 5 – first harmonic generator (FHG); 6 – quartz prism; 7 – filter; 8 – lens; 9 – photosensitive commutator, and 10 – registration plane. From ref. [10].

A primary unscattered electron beam is blocked by a Faraday cylinder, as in the standard continuous electron diffraction method. Required electron pulse lengths t_e and laser pulse length t_l depend on the character of the

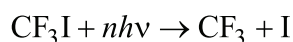
process being investigated. The duration of laser and electron pulses in the studies of coherent processes of nuclear dynamics must be part of the total time of the process, i.e., a snapshot in which events are averaged

over time t_c for obtaining ‘molecular movies’, with the exciting and probing pulses being generated by the same source. The controlled delay time between t_c and t_L denoted in the figure by t_d also depends on the character of the process being investigated [1, 2, 4, 133].

5.1. First experiments

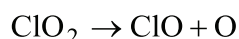
The first setup for studying structural dynamics and intermediate states of a chemical reaction by stroboscopic electron diffraction was designed in 1980 by a group of researchers of the Lomonosov Moscow State University and the Institute of Laser and Information Technologies, Russian Academy of Sciences (designated at that time as NITSTL AN SSSR). An electromagnetic lock was exploited in obtaining 20-ns long electron pulses.

The gaseous target (CF_3I molecules) was excited by a TEA CO_2 laser. Diffraction patterns of CF_3 free radicals (the products of multiphoton infrared (IR) dissociation of CF_3I molecules) were recorded for the first time:



It was crucial for experimental integrity in studies [1, 2] that almost 100% of the CF_3I molecules dissociated under the effect of a single 10^{-7} s IR laser pulse [134], yielding CF_3 radicals. This means that the diffraction pattern of scattering was recorded from the bulk (inside the IR laser beam caustic) containing no molecular components besides CF_3 ; the resulting diffraction pattern was unambiguously associated with CF_3 radicals. To record the diffraction pattern with the use of a secondary electron multiplier, the pulse-resonance method was employed [135, 136].

In 1984, paper [137] reported the application of stroboscopic electron diffraction for the study of ClO_2 photolysis with a resolution of ~ 1 ms:



To investigate coherent structural dynamics processes, an experimental setup was designed, in which a single pulse of an Nd:YAG laser with optical line-controlled delay was utilized to generate picosecond electron pulses and excite the target (Fig. 13).

The electron pulses were generated by the fourth harmonic of laser radiation 40 ps in duration at a wavelength of 266 nm. Electrons were ejected from the tip of a V-shaped tantalum cathode with a high quantum effectiveness $\sim 10^{-3}$ of the single-photon effect for the fourth harmonic and a slight excess of laser radiation energy over the cathode electron work function. At the same time, the initial alignment of the setup was also possible in the continuous electron beam thermoemission regime [4, 10, 133]. This apparatus was operated in the regime of generation of individual electron pulses

allowing one to measure the pulse lengths ($t_c \sim 100$ ps), and as a rectilinear scanning chamber to determine the mean number of electrons per single pulse ~ 1000 at a radiation power density 10^{10} W/cm² of the Nd:YAG laser. In addition, diffractograms of thin films made from polycrystalline zinc oxide were obtained. A comparison of electron diffraction patterns taken in pulsed and continuous beam regimes showed excellent agreement between them.

The present-day facilities used in the TRED method combine a few constituents, first and foremost a device generating femtosecond laser pulses and then ultrashort electron pulses; an electron-optical system forming electron bunches, synchronizing exciting laser pulses with diagnostic electron pulses; a system recording electron diffraction patterns with subsequent computer-assisted data collection and primary processing. Moreover, they contain systems for measuring pulse lengths and electron flux density, maintaining high vacuum (usually $\sim 10^{-6}$ Torr), and mass-spectral control of the study sample. Construction of such facilities began in the 1990s and thereafter depended on the degree of development of the relevant base of elements [10, 125].

5.2. Development of the time-resolved electron diffraction method

Further development of the TRED experiment is described in ref. [125]. The following elements were utilized: (1) a pulsed nozzle for injection of study matter, which favored marked enhancement of gas density in the scattering volume; (2) a system for amplification of the optical signal detected by a charge coupling device (CCD) camera that markedly increased the signal-to-noise ratio for a measured electron scattering intensity; (3) an internal standard (high-purity nitrogen molecules) for calibration of the diffraction pattern [83]. In this setup (Fig. 14), two synchronized pulses from a femtosecond laser are used for photogeneration of electrons and excitation of the object with the optical delay line between exciting and probing pulses.

The maximum concentration of scattering particles was reached by utilizing a pulsed nozzle for inputting gas into the diffraction chamber. The use of pulsed sources allowed the signal-to-noise ratio to be significantly improved by virtue of increased maximum concentration of particles in the scattering volume; simultaneously, the vacuum conditions were also improved. The combination of a pulsed source of gas supply and an ordinary effusion nozzle proved especially efficacious. In this device, the outlet opening of the pulsed nozzle was extended as a thin (0.2 mm) cylindrical channel, which allowed maintaining a high vacuum (10^{-6} Torr) and control concentration of molecules in the scattering volume at the nozzle edge, usually at a level of $10^{13} - 10^{16}$ mm⁻³. The use of the carrier gas for the injection of the study

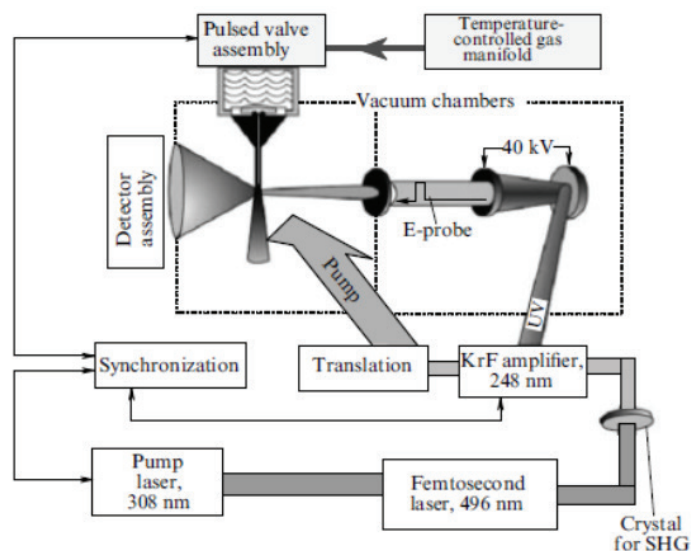


Fig. 14. Schematic of an experimental TRED setup. A 500-fs optical pulse (496 nm) is generated by a Lambda-Physics FAMP DFDL laser system, then the frequency is doubled by the second harmonic generator (SHG), and the resulting pulse (248 nm) is amplified as it passes twice through the synchronized krypton fluoride excimer laser, thus producing a subpicosecond pulse with an energy up to 10 mJ. Then, the beam is split by passing through controllable time-delay circuits to obtain pulses for the photoelectron sensor and optical pumping. From refs. [11,125] with minor revision.

substance through the pulsed nozzle permitted avoiding undesirable adiabatic cooling of the gas.

The authors of refs. [138, 139] designed a setup for generating ultrashort electron pulses with a high repetition rate (5 or 50 kHz). The pulses were emitted from a copper cathode. The second harmonic of a Ti:sapphire laser was utilized. The electrons were accelerated to 20 keV and intersected the effusion flux of the molecules of interest. The diffraction pattern was recorded by a CCD camera

cooled by liquid nitrogen. The molecular targets were excited by the 200-fs third-harmonic laser pulse at 265 nm (Fig. 15). The diffraction pattern was imposed on the luminophor and optically projected onto the CCD sensor [139]. The electron current intersecting the molecular beam was 20 pA, and corresponded to ~ 2500 electrons per pulse on the average, which reduced to a minimum pulse lengthening due to Coulomb repulsion (please see ref. [94]).

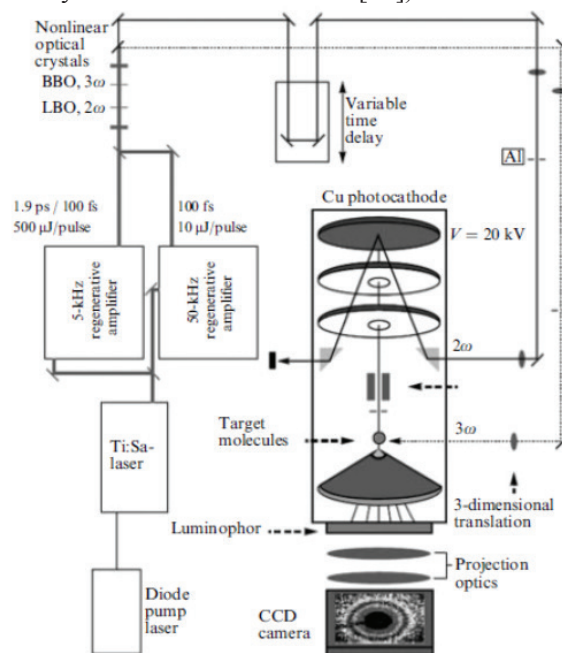


Fig. 15. The experimental TRED setup for generating ultrashort electron pulses with a high repetition rate (5 or 50 kHz). The pulses were emitted from a copper cathode. The second harmonic of a Ti:sapphire laser was utilized. The electrons were accelerated to 20 keV and intersected the effusion flux of the molecules of interest. The diffraction pattern was recorded by a CCD camera cooled by liquid nitrogen. From ref. [138].

It should be noted that any instability of laser radiation evolving during electron pulse generation is transformed into pulse instability. To minimize this effect, the laser radiation is focused on a diaphragm 200 mm in diameter. In this case, only the central part of the laser radiation is transmitted, while most of the second-harmonic power is lost. The diaphragm is mapped on the photocathode surface; therefore, the above instabilities of laser radiation are reduced to a minimum in the photocathode region from which electrons were generated. The quantum efficiency of photoemission is rather high, which makes it possible to reach an electron current of about 200 pA near the photocathode. To

decrease the influence of electron Coulomb repulsion, the current was lowered to 20 pA, when the beam traversed the diaphragm with a diameter of 30 mm in front of the target. The central beam of unscattered electrons was removed by a Faraday cylinder 375 mm in diameter. This apparatus was employed to study the structural dynamics of chemical reactions, in particular, the electrocyclic ring-opening reaction of 1,3-cyclohexadiene [138].

Fig. 16 displays a schematic of experimental arrangement for the study of ultrafast electron diffraction (UED). The diffraction chamber in this third-generation unit (UED-3) is coupled with a time-of-flight mass spectrometer (MS-TOF) [140].

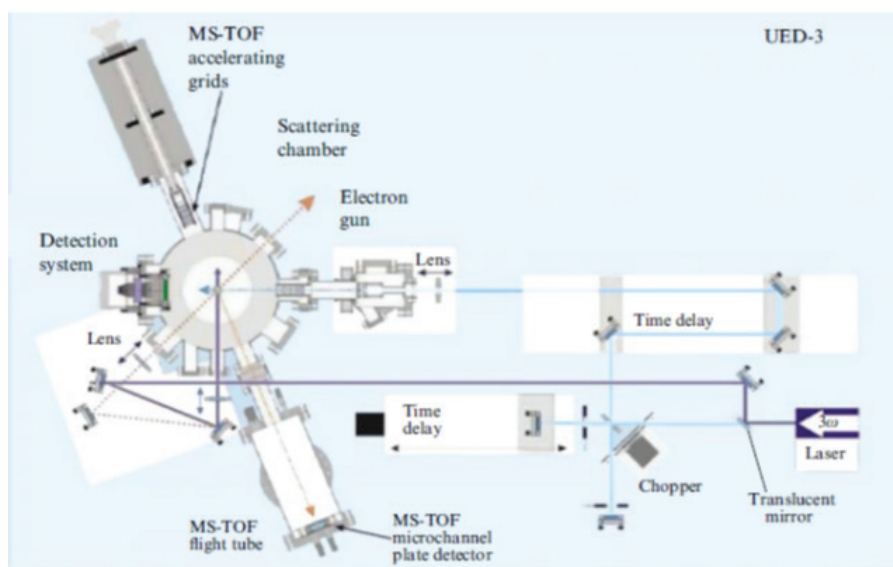


Fig. 16. Experimental Ultrafast Electron Diffraction (UED-3) setup coupled with a time-of-flight mass-spectrometer (MS-TOF), allowing for in situ control of the gas phase composition. From ref. [140].

The arrangement consists of four separate vacuum chambers, viz. an electron gun, scattering chamber, detection chamber, and MS-TOF for in situ control of the gas composition and detection of potentially corrosive compounds [140]. A vacuum at the level of $\sim 10^{-7}$ Torr is produced in the scattering chamber in the absence of a gas sample; the pressure builds up to 10^{-4} Torr when the molecules studied are introduced into the chamber. The pressure in the sensor chamber was maintained at the level of 10^{-2} Torr to avoid condensate formation on the thermoelectrically cooled surface. Special attention was given to avoiding parasitic electric or magnetic fields capable of distorting the trajectories of scattered electrons.

The detection system is of primary importance in the ultrafast electron diffraction method. The electron flux should be maintained at a very low level to ensure ultrafast temporal resolution of the system. The UED-3 apparatus contains a system for two-dimensional detection of the diffraction pattern based on a CCD matrix with a low noise level. Because scattering intensity in the course of electron diffraction rapidly decreases as the scattering

angle increases (by 6-8 orders of magnitude), a changeable symmetric optical filter representing an analog of the rotating sector in conventional gas electron diffraction is applied in the radial direction on the back wall of the scintillator [141]. Naturally, there are no moving mechanical parts here. The filter permits simultaneously measuring diffraction intensity over a dynamic range spanning more than seven orders of magnitude, which significantly increases the determination accuracy of structural parameters of the study sample. A typical UED experiment implies recording of 1000 frames per second for an exposition time 240 s (at a pulse repetition rate of 1 kHz). Averaging is performed over 100 diffraction patterns. Modern mathematical methods are applied to process signals as described in [142]. A series of studies on the dynamics of free molecules and transition states of chemical reactions were carried out at UED-3 facility (see [140] for details).

Recently a new femtosecond electron diffraction apparatus with time resolution of ~ 300 fs was developed [143]. The scheme of the experimental setup used in our experiments and implementing the TRED method is

shown in Fig. 17. The main frequency of a femtosecond Ti:sapphire laser ($\lambda_1 = 800$ nm) was used as the pump beam and the photoelectron beam formed under the irradiation of the semitransparent photocathode with the third harmonic of the Ti:sapphire laser ($\lambda_2 = 266$ nm) was used as the probe beam. In this manner, the optical and photoelectron pulses were strictly synchronized. The laser pulse duration was 50 fs. The pulse repetition frequency was 1 kHz. The photocathode material was a silver layer with a thickness of ~ 30 nm deposited on a thin quartz plate. The studied sample was an antimony film with a thickness of about 30 nm prepared by thermal deposition in vacuum on a standard carbon substrate with a thickness of 20–30 nm used in transmission electron microscopes. The

pump laser radiation was incident on the sample at an angle of 45° . The energy density in the laser beam on the sample surface was 1.5 mJ/cm². Such radiation energy density made it possible to perform rather long-term measurements without noticeable degradation of the sample. The kinetic energy of probe photoelectrons was 20 keV. The diameter of the electron beam in the region of the sample was ~ 0.1 mm. A lens based on a constant magnet adapted for the given energy of the electron beam served as a focusing system that made it possible to minimize the time-of-flight interval of electrons. The sample-diffracted electron beam amplified on the detector using microchannel plates got to the luminophore and was detected on a CCD camera (Fig. 17).

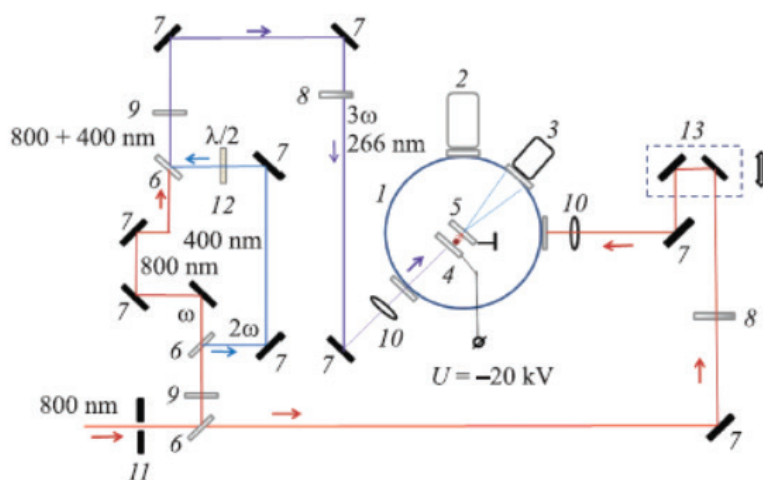


Fig. 17. Experimental scheme of the femtosecond TRED apparatus: (1) vacuum chamber, (2) turbomolecular pump, (3) amplifier of the electron current on the basis of microchannel plates and CCD chamber, (4) silver photocathode, (5) anode and target, (6) beam splitters, (7) mirrors, (8) radiation attenuator, (9) converters into the second and third harmonics, (10) lenses, (11) diaphragm, (12) polarization rotator, and (13) delay line. From ref. [143].

The main frequency of a femtosecond Ti:sapphire laser ($\lambda_1 = 800$ nm) was used as the pump beam and the photoelectron beam formed under the irradiation of the semitransparent photocathode with the third harmonic of the Ti:sapphire laser ($\lambda_2 = 266$ nm) was used as the probe beam. In this manner, the optical and photoelectron pulses were strictly synchronized. The laser pulse duration was 50 fs. The pulse repetition frequency was 1 kHz. The photocathode material was a silver layer with a thickness of ~ 30 nm deposited on a thin quartz plate. The studied sample was an antimony film with a thickness of about 30 nm prepared by thermal deposition in vacuum on a standard carbon substrate with a thickness of 20–30 nm used in transmission electron microscopes. The pump laser radiation was incident on the sample at an angle of 45° . The energy density in the laser beam on the sample surface was 1.5 mJ/cm². Such radiation energy density made it possible to perform rather long-term measurements without noticeable degradation of the sample. The kinetic energy of probe photoelectrons was

20 keV. The diameter of the electron beam in the region of the sample was ~ 0.1 mm. A lens based on a constant magnet adapted for the given energy of the electron beam served as a focusing system that made it possible to minimize the time-of-flight interval of electrons. The sample-diffracted electron beam amplified on the detector using microchannel plates got to the luminophore and was detected on a CCD camera. A general view of the apparatus is shown in Fig. 18.

The generation of coherent optical phonons in an antimony film has been directly observed by the femtosecond electron diffraction method. The sample has been excited by a femtosecond laser pulse ($\lambda = 800$ nm) and probed with a pulsed photoelectron beam. Oscillations of the intensity corresponding to vibration frequencies of optical phonons excited by the laser have been observed in the obtained diffraction patterns: totally symmetric (A_{1g}) and twofold degenerate (E_{2g}) phonon modes of antimony and their combinations [143]. The details of this study will be described in the Part III of our article.

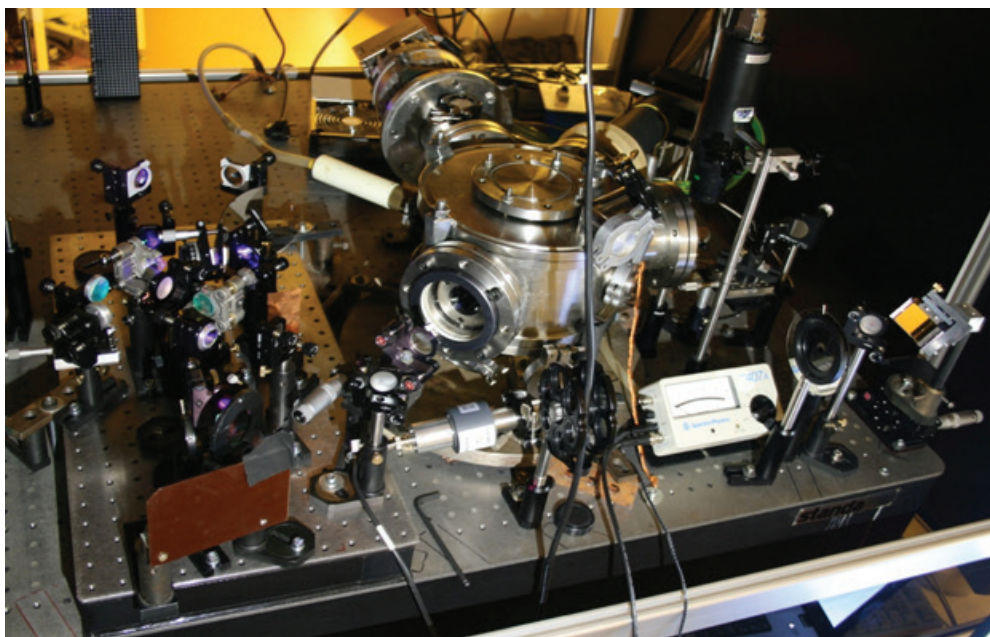


Fig. 18. General view of the femtosecond electron diffraction setup developed by research groups from the Institute of Spectroscopy, RAS and Moscow Technological University, Institute of Fine Chemical Technologies. From ref. [143].

Concluding remarks: future outlook

The development of appropriate experimental facilities for time-resolved electron diffraction and electron microscopy [144] made it possible to combine a spatial resolution on the order of $\sim 10^{-2} - 10^{-3}$ Å with pico- and even subpicosecond temporal resolution into a single complex. Some authors have reported the generation of ~ 200 -fs electron pulses [145–151]. The preparation of 10 fs long pulses containing $10^4 - 10^6$ electrons in future research would be of paramount importance for the observation of fast processes in matter and concomitant changes in its structure. Also needed is an effective method for the reliable measurement of such short temporal characteristics of electron bunches [145].

The present review is concerned with processes studied with the aid of modern sources of femtosecond laser radiation on a time scale from nano- to femtoseconds or shorter extending even to the subfemtosecond (attosecond) region. The reader may ask: is it possible to make use of ultrafast electron diffraction in studying very short (say, shorter than 1 as) processes? In principle, such studies can be conducted in the case of diffraction of isolated relativistic electrons scattered with the characteristic time $\tau \sim D(\text{nucleus})/c = 10^{-22} - 10^{-23}$ s. Under favorable conditions, the results may open up new possibilities for the investigation of the dynamics of extreme states of matter [152]. Naturally, the development of such a new promising line of research will require great efforts by both experimentalists and theorists, as well as considerable financial investments, let alone the proper experimental base. It can be expected

that the success of these activities will depend on how effectively the methods and approaches from different fields of physics and technology are combined into a single experimental layout [153, 154]. It cannot be ruled out that a combination of two different type microscopes [144], namely, an electron microscope and, for example, a scanning probe microscope, in a single experimental layout may turn out well justified to improve the characteristics of a unique measuring device as a whole, as described in [155]. It is worth mentioning an original method of scanning vacuum probe microscopy with a hollow tip, the development of which is underway at the Institute of Spectroscopy, Russian Academy of Sciences [156]. Such a tip, a dielectric or microcapillary coated with a thin metallic layer, may have a 100-nm aperture (commercial variant) or a 10-nm open hole (laboratory design) [157]. This instrument is expected to enable modification of surfaces with ion and electron microbeams or soft X-ray radiation directed to the sample through the capillary, and investigation of surface molecular complexes by passing photoions or photoelectrons through the scanning hollow tip. In the photoionic mode, time-of-flight mass spectrometry will make it possible to realize nanolocal photodesorption of molecular ions when high spatial resolution is combined with high chemical, elemental selectivity. This method may add information about a sample to that obtained with an electron microscope. We appear to be witnessing not only the new birth of electron microscopy, but also its principally new achievements to come as it approaches the centenary of successful developments and wide practical applications. Today, it provides the principal possibility of studying the properties of matter in the

space-time continuum exploiting short photoelectron beams. Characteristically, there are 30 – 40 research laboratories all over the world experimenting or planning to experiment with ultrafast electron diffraction [158] and one tenth that number of centers

possessing electron microscopes adapted to operate with ultrashort electron beams.

Acknowledgements. *This work supported by RFBR grant No. 16-29-1167 OFI_m and partially by RFBR grant No. 14-22-02035 OFI_m.*

References:

1. Ischenko A.A. [et al.] A stroboscopic gas-electron diffraction method for the investigation of short-lived molecular species // *Appl. Phys. B Photophysics Laser Chem.* 1983. V. 32, № 3. P. 161–163.
2. Ischenko A.A. [et al.] The observation of electron diffraction from free radicals – products of the IR multiphoton dissociation of CF₃I molecules by stroboscopic gas electron diffraction // *Bull. Moscow Univ. Ser 2. Chem.* 1985. V. 26, № 2. P. 140–143.
3. Ischenko A.A. [et al.] The study of short-lived intermediate species and structural kinetics of photoexcited molecules by stroboscopic electron diffraction // *Interuniversity collection of scientific papers. The Structure and Properties of Molecules.* Ivanovo, 1988. P. 63–77.
4. Vabishchevich M.G., Ischenko A.A. Method of studying the kinetics of fast processes; USSR Certificate number 1679907. Registered in the State Register of Inventions of the USSR on May 22, 1991. Priority of invention October 14, 1988.
5. Norrish R.G.W., Porter G. Chemical reactions produced by very high light intensities // *Nature.* 1949. V. 164, № 4172. P. 658–658.
6. Tomov I.V. [et al.] Picosecond hard X-ray pulses and their application to time-resolved diffraction // *Time-resolved diffraction* / ed. Helliwell J.R., Rentzepis P.M. Oxford: Clarendon Press, 1997. P. 1–43.
7. Ischenko A.A., Girichev G.V., Tarasov Y.I. Electron diffraction: structure and dynamics of free molecules and condensed matter. Moscow: FIZMATLIT, 2013. 616 p.
8. Ischenko A.A., Aseyev S.A. Time resolved electron diffraction: for chemistry, biology and material science. San Diego: Elsevier, 2014. 310 p.
9. Minitti M.P. [et al.] Toward structural femtosecond chemical dynamics: imaging chemistry in space and time // *Faraday Discuss.* 2014. V. 171. P. 81–91.
10. Ischenko A.A. [et al.] The stroboscopic gas electron diffraction method for investigation of time-resolved structural kinetics in photoexcitation processes // *J. Mol. Struct. Elsevier*, 1993. V. 300. P. 115–140.
11. Ewbank J.D., Schäfer L., Ischenko A.A. Structural and vibrational kinetics of photoexcitation processes using time resolved electron diffraction // *J. Mol. Struct.* 2000. V. 524, № 1. P. 1–49.
12. Ruan C.-Y. [et al.] The Development and Applications of Ultrafast Electron Nanocrystallography // *Microsc. Microanal.* 2009. V. 15, № 4. P. 323–337.
13. Weber P.M., Carpenter S.D., Lucza T. Reflectron design for femtosecond electron guns // *Proc. SPIE 2521, Time-Resolved Electron and X-Ray Diffraction*, 23 (September 1, 1995) / ed. Rentzepis P.M. 1995. № 2521. P. 23–30.
14. King W.E. [et al.] Ultrafast electron microscopy in materials science, biology, and chemistry // *J. Appl. Phys.* 2005. V. 97, № 11. P. 111101, 1–27.
15. Zewail A.H. Ultrafast electron diffraction, crystallography, and microscopy // *Annu. Rev. Phys. Chem.* 2006. V. 57, № 1. P. 65–103.
16. Zewail A.H. Four-dimensional electron microscopy // *Science (80-)*. 2010. V. 328, № 5975. P. 187–193.
17. Zewail A.H., Thomas J.M. 4D electron microscopy. Imaging in space and time. Imperial College Press, 2010. 360 p.
18. Ischenko A.A. Molecular tomography of the quantum state by time-resolved electron diffraction // *Phys. Res. Int.* 2013. V. 2013. P. 1–8.
19. Sciaini G., Miller R.J.D. Femtosecond electron diffraction: heralding the era of atomically resolved dynamics // *Reports Prog. Phys.* 2011. V. 74, № 9. P. 096101 (1–36).
20. Ischenko A.A., Bagratashvili V.N., Avilov A.S. Methods for studying the coherent 4D structural dynamics of free molecules and condensed state of matter: article // *Crystallogr. Reports.* 2011. V. 56, № 5. P. 751.
21. Miller R.J.D. Mapping atomic motions with ultrabright electrons: the chemists' gedanken experiment enters the lab frame // *Annu. Rev. Phys. Chem.* 2014. V. 65, № 1. P. 583–604.
22. Miller R.J.D. Femtosecond crystallography with ultrabright electrons and X-rays: capturing chemistry in action // *Science (80-)*. 2014. V. 343, № 6175. P. 1108–1116.
23. Ischenko A.A. [et al.] Ultrafast electron diffraction and electron microscopy: present status and future prospects // *Physics-Uspekhi.* 2014. V. 57, № 7. P. 633–669.
24. Campbell G.H., McKeown J.T., Santala M.K. Time resolved electron microscopy for in situ experiments // *Appl. Phys. Rev.* 2014. V. 1, № 4. P. 41101.
25. Kim K.T., Villeneuve D.M., Corkum P.B. Manipulating quantum paths for novel attosecond measurement methods // *Nat. Photonics.* 2014. V. 8, № 3. P. 187–194.
26. Petek H. Single-molecule femtochemistry:

molecular imaging at the space-time limit // *ACS Nano*. 2014. V. 8, № 1. P. 5–13.

27. Manz S. [et al.] Mapping atomic motions with ultrabright electrons: towards fundamental limits in space-time resolution // *Faraday Discuss.* 2015. V. 177. P. 467–491.

28. Robinson M.S., Lane P.D., Wann D.A. A compact electron gun for time-resolved electron diffraction // *Rev. Sci. Instrum.* 2015. V. 86, № 1. P. 13109.

29. Plemmons D.A., Suri P.K., Flannigan D.J. Probing structural and electronic dynamics with ultrafast electron microscopy // *Chem. Mater.* 2015. V. 27, № 9. P. 3178–3192.

30. Bonham R.A., Fink M. High energy electron scattering. New York: Van Nostrand Reinhold, 1974. 311 p.

31. Hargittai I. The gas-phase electron diffraction technique of molecular structure determination // *Stereochemical applications of gas-phase electron diffraction. Part A. The electron diffraction technique / ed. Hargittai I., Hargittai M.* New York: VCH, 1988. P. 1–54.

32. Ischenko A.A., Schäfer L., Ewbank J.D. Structural kinetics by time-resolved gas electron diffraction: coherent nuclear dynamics in laser excited spatially anisotropic molecular ensembles // *J. Mol. Struct.* 1996. V. 376, № 1-3. P. 157–171.

33. Ischenko A.A., Schäfer L., Ewbank J. Time-resolved electron diffraction: a method to study the structural vibrational kinetics of photoexcited molecules // *Time-resolved diffraction 13 / ed. Helliwell J.R., Rentzepis P.M.* Oxford University Press, 1997. P. 323–390.

34. Debye P. The influence of intramolecular atomic motion on electron diffraction diagrams // *J. Chem. Phys.* 1941. V. 9, № 1. P. 55–60.

35. Bialynicki-Birula I. [et al.] *Theory of quanta*. New York: Oxford University Press, 1992. 494 p.

36. Cohen-Tannoudji C., Diu B., Laloë F. *Quantum mechanics*. V. 1. Wiley, 1977. 914 p.

37. Ewbank J.D., Schäfer L., Ischenko A.A. Structural kinetics by stroboscopic gas electron diffraction 2. Time-dependent molecular intensities of predissociation processes // *J. Mol. Struct.* Elsevier, 1994. V. 321, № 3. P. 265–278.

38. Tikhonov A.N., Arsenin V.Y. *Solution of the ill-posed problems*. New York: Halsted Press, 1977. 256 p.

39. Ryu S., Weber P.M., Stratt R.M. The diffraction signatures of individual vibrational modes in polyatomic molecules // *J. Chem. Phys.* 2000. V. 112, № 3. P. 1260–1270.

40. Ryu S., Stratt R.M., Weber P.M. Diffraction signals of aligned molecules in the gas phase: tetrazine in intense laser fields // *J. Phys. Chem. A*. 2003. V. 107, № 34. P. 6622–6629.

41. Ryu S. [et al.] Electron diffraction of molecules in specific quantum states: a theoretical study of

vibronically excited s-tetrazine // *J. Phys. Chem. A*. 2004. V. 108, № 7. P. 1189–1199.

42. Weber P.M. [et al.] Experimental and theoretical studies of pump-probe electron diffraction: time-dependent and state-specific signatures in small cyclic molecules // *Femtochemistry and Femtobiology*. Elsevier, 2004. P. 19–24.

43. Zewail A.H. *Femtochemistry: ultrafast dynamics of the chemical bond*. World Scientific Publishing Company, 1994. V. 3.

44. Zewail A.H. Femtochemistry: recent progress in studies of dynamics and control of reactions and their transition states // *J. Phys. Chem.* 1996. V. 100, № 31. P. 12701–12724.

45. Zewail A.H. Femtochemistry: atomic-scale dynamics of the chemical bond using ultrafast lasers (Nobel Lecture) // *Angew. Chem. Int. Ed. Engl.* 2000. V. 39, № 15. P. 2586–2631.

46. Zewail A.H. Femtochemistry: atomic-scale dynamics of the chemical bond // *J. Phys. Chem. A. American Chemical Society*. 2000. V. 104, № 24. P. 5660–5694.

47. Buchachenko A.L. Chemistry on the border of two centuries – achievements and prospects // *Russ. Chem. Rev.* 1999. V. 68, № 2. P. 85–102.

48. Neutze R. [et al.] Potential for biomolecular imaging with femtosecond X-ray pulses // *Nature*. 2000. V. 406, № 6797. P. 752–757.

49. Chapman H.N. [et al.] Femtosecond diffractive imaging with a soft-X-ray free-electron laser // *Nat. Phys.* 2006. V. 2, № 12. P. 839–843.

50. Bogan M.J. [et al.] Single particle X-ray diffractive imaging // *Nano Lett.* 2008. V. 8, № 1. P. 310–316.

51. Bogan M.J. [et al.] Single-particle coherent diffractive imaging with a soft X-ray free electron laser: towards soot aerosol morphology: *JOUR // J. Phys. B. At. Mol. Opt. Phys.* 2010. V. 43, № 19. P. 194013.

52. Yoon C.H. [et al.] Unsupervised classification of single-particle X-ray diffraction snapshots by spectral clustering // *Opt. Express*. 2011. V. 19, № 17. P. 16542–16549.

53. Baskin J.S., Zewail A.H. Ultrafast electron diffraction: oriented molecular structures in space and time // *ChemPhysChem*. 2005. V. 6, № 11. P. 2261–2276.

54. Williamson J.C., Zewail A.H. Ultrafast electron diffraction. 4. Molecular structures and coherent dynamics // *J. Phys. Chem.* 1994. V. 98, № 11. P. 2766–2781.

55. Hoshina K. [et al.] Direct observation of molecular alignment in an intense laser field by pulsed gas electron diffraction I: observation of anisotropic diffraction image // *Chem. Phys. Lett.* 2002. V. 353, № 1–2. P. 27–32.

56. Hoshina K. [et al.] Direct observation of molecular alignment in an intense laser field by pulsed gas electron diffraction II: analysis of anisotropic diffraction image // *Chem. Phys. Lett.* 2002. V. 353,

№ 1-2. P. 33–39.

57. Hoshina K. [et al.] Alignment of CS₂ in intense nanosecond laser fields probed by pulsed gas electron diffraction // *J. Chem. Phys.* 2003. V. 118, № 14. P. 6211–6221.

58. Spence J.C.H., Doak R.B. Single molecule diffraction // *Phys. Rev. Lett.* 2004. V. 92, № 19. P. 198102 (1-4).

59. Reckenthaeler P. [et al.] Time-resolved electron diffraction from selectively aligned molecules // *Phys. Rev. Lett.* 2009. V. 102, № 21. P. 213001–213004.

60. Bergsma J.P. [et al.] Transient X-ray scattering calculated from molecular dynamics // *J. Chem. Phys.* 1986. V. 84, № 11. P. 6151–6160.

61. Zare R.N. Angular momentum: understanding spatial aspects in chemistry and physics // *Physics Today*. New York: Wiley, 1988. 349 p.

62. Choi S.E., Bernstein R.B. Theory of oriented symmetric-top molecule beams: Precession, degree of orientation, and photofragmentation of rotationally state-selected molecules // *J. Chem. Phys.* 1986. V. 85, № 1. P. 150–161.

63. Gradstein I.S., Ryzhik I.M. Table of integrals, series, and products. New York: Academic Press, 2014. 1184 p.

64. Handbook of mathematical functions with formulas, graphs, and mathematical tables / ed. Abramowitz M., Stegun I.A. Washington, D.C.: National Bureau of Standards, 1965. 1058 p.

65. Vetchinkin S.I. [et al.] Gaussian wavepacket dynamics in an anharmonic system // *Chem. Phys. Lett.* 1993. V. 215, № 1–3. P. 11–16.

66. Eryomin V.V., Kuz'menko N.E., Umanskii I.M. Interference effects in wave packet dynamics at the pulse optical excitation of a diatomic molecule // *Russ. J. Phys. Chem. B (Khimicheskaya Fizika)* 1996. V. 15, № 5. P. 5–12 (in Russ.).

67. Kosloff R. Time-dependent quantum-mechanical methods for molecular dynamics // *J. Phys. Chem.* 1988. V. 92, № 8. P. 2087–2100.

68. Kosloff R. [et al.] Wavepacket dancing: Achieving chemical selectivity by shaping light pulses // *Chem. Phys.* 1989. V. 139, № 1. P. 201–220.

69. Balint-Kurti G.G., Dixon R.N., Marston C.C. Grid methods for solving the Schrödinger equation and time dependent quantum dynamics of molecular photofragmentation and reactive scattering processes // *Int. Rev. Phys. Chem.* 1992. V. 11, № 2. P. 317–344.

70. Stolow A., Underwood J.G. Time-resolved photoelectron spectroscopy of nonadiabatic dynamics in polyatomic molecules // *Advances in Chemical Physics*, Volume 139 / ed. Rice S.A. John Wiley & Sons, Inc., Hoboken, NJ, USA, 2008. P. 497–584.

71. Rapp D., Kassal T. Theory of vibrational energy transfer between simple molecules in nonreactive

collisions // *Chem. Rev.* 1969. V. 69, № 1. P. 61–102.

72. Levine R.D. Molecular reaction dynamics: book. Cambridge University Press, 2009. 555 p.

73. Herzberg G. Molecular spectra and molecular structure. III. Electronic spectra and electronic structure of polyatomic molecules: book. Van Nostrand, 1966. 784 p.

74. Rosker M.J., Dantus M., Zewail A.H. Femtosecond real-time probing of reactions. I. The technique // *J. Chem. Phys.* 1988. V. 89, № 10. P. 6113–6127.

75. Khundkar L.R., Zewail A.H. Ultrafast molecular reaction dynamics in real-time: Progress over a decade // *Annu. Rev. Phys. Chem.* 1990. V. 41, № 1. P. 15–60.

76. Okabe H. Photochemistry of small molecules: book. Wiley, 1978.

77. Baronavski A.P. Laser ultraviolet photochemistry: book // *Lasers as reactants and probes in chemistry* / ed. Jackson W.M., Harvey A.B. Washington, D.C.: Howard University Press, 1985. P. 81.

78. Stereochemical applications of gas-phase electron diffraction. Part A. The electron diffraction technique: book / ed. Hargittai I., Hargittai M. VCH Publishers, 1988.

79. Garraway B.M., Suominen K.-A. Wave-packet dynamics: new physics and chemistry in femto-time // *Reports Prog. Phys.* 1995. V. 58, № 4. P. 365–419.

80. Heller E.J. Time-dependent approach to semiclassical dynamics // *J. Chem. Phys.* 1975. V. 62, № 4. P. 1544–1555.

81. Heller E.J. Potential surface properties and dynamics from molecular spectra: a time-dependent picture // *Potential energy surfaces and dynamics calculations*. Boston, MA: Springer US, 1981. P. 103–131.

82. Heller E.J. Quantum localization and the rate of exploration of phase space // *Phys. Rev. A* 1987. V. 35, № 3. P. 1360–1370.

83. Ischenko A.A., Ewbank J.D., Schäfer L. Structural kinetics by stroboscopic gas electron diffraction Part 1. Time-dependent molecular intensities of dissociative states // *J. Mol. Struct.* 1994. V. 320. P. 147–158.

84. Schafer L. [et al.] Photodissociation dynamics of randomly oriented molecular ensembles by time-resolved electron diffraction // *Izv. Vyss. Uchebn. Zaved. Khim. Khim. Tekhnol.* 2016. V. 59, № 12. P. 22–31 (in Russ.).

85. Kemble E.C. The fundamental principles of quantum mechanics: with elementary applications: book. Dover Publications, 2005. 611 p.

86. Ballentine L.E. Quantum mechanics. A modern development. Singapore: World Scientific Publishing Co. Pte. Ltd., 1998. 658 p.

87. Wigner E. On the quantum correction for thermodynamic equilibrium // *Phys. Rev.* 1932. V. 40, № 5. P. 749–759.

88. Yourgrau W., Van Der Merwe A., Landé A. Perspectives in quantum theory: book. Dover Publ., 1979. 283 p.
89. Hillery M. [et al.] Distribution functions in physics: fundamentals // *Phys. Rep.* 1984. V. 106, № 3. P. 121–167.
90. Hillery M. [et al.] Distribution functions in physics: fundamentals: in book // Part I: Physical Chemistry. Part II: Solid State Physics / ed. Wightman A.S. Berlin, Heidelberg: Springer Berlin Heidelberg, 1997. P. 273–317.
91. Cahill K.E., Glauber R.J. Density operators and quasiprobability distributions // *Phys. Rev.* 1969. V. 177, № 5. P. 1882–1902.
92. Freenberg E. The scattering of slow electrons in neutral atoms. Harvard University, 1933. 125 p.
93. Weigert S. How to determine a quantum state by measurements: The Pauli problem for a particle with arbitrary potential // *Phys. Rev. A.* 1996. V. 53, № 4. P. 2078–2083.
94. Williamson J.C. [et al.] Clocking transient chemical changes by ultrafast electron diffraction: *JOUR // Nature.* 1997. V. 386, № 6621. P. 159–162.
95. Ihee H., Zewail A.H., Goddard W.A. Conformations and barriers of haloethyl radicals (CH_2XCH_2 , X = F, Cl, Br, I): Ab Initio Studies // *J. Phys. Chem. A.* 1999. V. 103, № 33. P. 6638–6649.
96. Ihee H., Kua J., Zewail A.H. $\text{CF}_2\text{XCF}_2\text{X}$ and $\text{CF}_2\text{XCF}_2 \cdot$ radicals (X = Cl, Br, I): ab initio and DFT studies and comparison with experiments // *J. Phys. Chem. A.* 2001. V. 105, № 14. P. 3623–3632.
97. Tannor D.J., Rice S.A. Control of selectivity of chemical reaction via control of wave packet evolution // *J. Chem. Phys.* 1985. V. 83, № 10. P. 5013–5018.
98. Yan Y.J., Mukamel S. Femtosecond pump-probe spectroscopy of polyatomic molecules in condensed phases // *Phys. Rev. A.* 1990. V. 41, № 11. P. 6485–6504.
99. Yan Y.J. [et al.] Optical control of molecular dynamics: Liouville-space theory // *J. Phys. Chem.* 1993. V. 97, № 10. P. 2320–2333.
100. Krause J.L. [et al.] Optical control of molecular dynamics: Molecular cannons, reflectrons, and wave-packet focusers // *J. Chem. Phys.* 1993. V. 99, № 9. P. 6562–6578.
101. Krause J.L. [et al.] Light packet control of wave packet dynamics // *Femtosecond Chemistry* / ed. Manz J., Woste L. Weinheim: VCH Publishers, 1995. P. 743–779.
102. Krause J.L. [et al.] Creating and detecting shaped rydberg wave packets // *Phys. Rev. Lett.* 1997. V. 79, № 25. P. 4978–4981.
103. Ischenko A.A., Ewbank J.D., Schäfer L. Structural and vibrational kinetics by time-resolved gas electron diffraction: stochastic approach to data analysis // *J. Phys. Chem.* 1995. V. 99, № 43. P. 15790–15797.
104. Leonhardt U. State reconstruction of anharmonic molecular vibrations: Morse-oscillator model // *Phys. Rev. A.* 1997. V. 55, № 4. P. 3164–3172.
105. Ischenko A.A. The study of coherent dynamics of the nuclei by time-resolved electron diffraction. II. The scattering of electrons by coherently excited molecules // *Russ. Trans. Chem. Chem. Technol.* 2009. V. 52, № 8. P. 59–63.
106. Ischenko A.A. The study of coherent dynamics of the nuclei by time-resolved electron diffraction. III. Molecular quantum state tomography // *Russ. Trans. Chem. Chem. Technol.* 2009. V. 52, № 9. P. 62–66.
107. Natterer F. The mathematics of computerized tomography: book. Vieweg+Teubner Verlag, 2013. 222 p.
108. Leonhardt U. Discrete Wigner function and quantum-state tomography. // *Phys. Rev. A, At. Mol. Opt. Phys.* 1996. V. 53, № 5. P. 2998–3013.
109. Leonhardt U. Measuring the quantum state of light. Cambridge: Cambridge University Press, 1997. 208 p.
110. Munroe [et al.] Photon-number statistics from the phase-averaged quadrature-field distribution: Theory and ultrafast measurement. // *Phys. Rev. A, At. Mol. Opt. Phys.* 1995. V. 52, № 2. P. R924–R927.
111. de Groot S.R., Suttrop L.G. Foundations of electrodynamics: book. North-Holland, 1972. 535 p.
112. Richter T. Pattern functions used in tomographic reconstruction of photon statistics revisited // *Phys. Lett. A.* 1996. V. 211, № 6. P. 327–330.
113. Richter T. Direct sampling of a smoothed Wigner function from quadrature distributions // *J. Opt. B Quantum Semiclassical Opt.* 1999. V. 1, № 6. P. 650–654.
114. Richter T., Wünsche A. Determination of quantum state from time-dependent position distributions // *Acta Phys. Slovaca.* 1996. V. 46. P. 487–494.
115. Leonhardt U. [et al.] Sampling of photon statistics and density matrix using homodyne detection // *Opt. Commun.* 1996. V. 127, № 1–3. P. 144–160.
116. Leonhardt U., Raymer M.G. Observation of moving wave packets reveals their quantum state // *Phys. Rev. Lett.* 1996. V. 76, № 12. P. 1985–1989.
117. Leonhardt U., Schneider S. State reconstruction in one-dimensional quantum mechanics: The continuous spectrum // *Phys. Rev. A.* 1997. V. 56, № 4. P. 2549–2556.
118. Leonhardt U. Optical conformal mapping // *Science (80-)*. 2006. V. 312, № 5781. P. 1777–1780.
119. Messiah A. Quantum mechanics: book. Dover Publications, 2014. 1152 p.
120. Ischenko A.A., Schäfer L., Ewbank J.D. Manifestation of chaotic nuclear dynamics of highly excited polyatomic molecules in time-resolved electron diffraction data // *J. Phys. Chem. A.* 1998. V. 102, № 37. P. 7329–7332.

121. Todd T.R., Olson W.B. The infrared spectra of $^{12}\text{C}^{32}\text{S}$, $^{12}\text{C}^{34}\text{S}$, $^{13}\text{C}^{32}\text{S}$, and $^{12}\text{C}^{33}\text{S}$ // *J. Mol. Spectrosc.* 1979. V. 74, № 2. P. 190–202.
122. Tzeng W.-B. [et al.] A 193 nm laser photofragmentation time-of-flight mass spectrometric study of CS_2 and CS_2 clusters // *J. Chem. Phys.* 1988. V. 88, № 3. P. 1658–1669.
123. Ischenko A.A. [et al.] Stroboscopic gas electron diffraction: a tool for structural kinetic studies of laser-excited molecules // *Time-Resolved Electron and X-Ray Diffraction*, v. 2521 / ed. Rentzepis P.M. 1995. P. 123–135.
124. Schelev M.Y. 500-fs photoelectron gun for time-resolved electron diffraction experiments // *Opt. Eng.* 1998. V. 37, № 8. P. 2249–2254.
125. Lobastov V.A. [et al.] Instrumentation for time-resolved electron diffraction spanning the time domain from microseconds to picoseconds // *Rev. Sci. Instrum.* 1998. V. 69, № 7. P. 2633–2643.
126. Hebeisen C.T. [et al.] Femtosecond electron pulse characterization using laser ponderomotive scattering // *Opt. Lett.* 2006. V. 31, № 23. P. 3517–3520.
127. Hebeisen C.T. [et al.] Grating enhanced ponderomotive scattering for visualization and full characterization of femtosecond electron pulses // *Opt. Express*. 2008. V. 16, № 5. P. 3334–3341.
128. Hebeisen C.T. [et al.] Characterization of ultrashort electron pulses: in book // *Ultrafast Phenomena XV: Proceedings of the 15th Int. Conference*, Pacific Grove, USA, July 30 – August 4, 2006 / ed. Corkum P. [et al.] Berlin, Heidelberg: Springer-Verlag Berlin Heidelberg, 2007. P. 758–760.
129. Gahlmann A., Tae Park S., Zewail A.H. Ultrashort electron pulses for diffraction, crystallography and microscopy: theoretical and experimental resolutions // *Phys. Chem. Chem. Phys.* 2008. V. 10, № 20. P. 2894.
130. Glinec Y. [et al.] Generation of quasi-monoenergetic electron beams using ultrashort and ultraintense laser pulses // *Laser Part. Beams*. 2005. V. 23, № 2.
131. Hommelhoff P. [et al.] Field emission tip as a nanometer source of free electron femtosecond pulses // *Phys. Rev. Lett.* 2006. V. 96, № 7. P. 77401.
132. Tellinghuisen J. Potentials for weakly bound states in I_2 from diffuse spectra and predissociation data // *J. Chem. Phys.* 1985. V. 82, № 9. P. 4012–4016.
133. Akhmanov S.A. [et al.] Generation of the picosecond electron pulses of fast electrons in the EMR-100 electron diffraction apparatus by photoemission in the laser field // *Russ. J. Techn. Phys. Lett.* 1985. V. 11, № 3. P. 157–161.
134. Bagratashvili V.N. [et al.] Isotopic selectivity of IR laser photodissociation of CF_3I molecules // *Appl. Phys.* 1979. V. 20, № 3. P. 231–235.
135. Golubkov V. V. [et al.] Pulse-resonance signal method for the recording of signal in a stroboscopic electron microscopy // XII Vsesoyuz. Konf. po Elektronnoi Mikroskopii, Sumy, Oktyabr' 1982. Tezisy Dokladov (XII All-Union Conf. on Electron Microscopy, Sumy, October 1982, Abstracts). Moscow: Nauka, 1982. P. 62 (in Russ.).
136. Golubkov V. V. [et al.] New methods for the registration of the signal in gas electron diffraction // *Izv. Akad. Nauk SSSR Ser. Fiz.* 1983. V. 47. P. 1115–1121 (in Russ.).
137. Rood A.P., Milledge J. Combined flash-photolysis and gas-phase electron-diffraction studies of small molecules // *J. Chem. Soc. Faraday Trans. 2*. 1984. V. 80, № 9. P. 1145–1153.
138. Dudek R.C., Weber P.M. Ultrafast diffraction imaging of the electrocyclic ring-opening reaction of 1,3-cyclohexadiene // *J. Phys. Chem. A. American Chemical Society*. 2001. V. 105, № 17. P. 4167–4171.
139. Cardoza J.D. [et al.] Centering of ultrafast time-resolved pump-probe electron diffraction patterns // *Chem. Phys.* 2004. V. 299, № 2–3. P. 307–312.
140. Srinivasan R. [et al.] Ultrafast electron diffraction (UED) // *Helv. Chim. Acta*. 2003. V. 86, № 6. P. 1761–1799.
141. Goodman P. Fifty years of electron diffraction: in recognition of fifty years of achievement by the crystallographers and gas diffractionists in the field of electron diffraction: book / Published for the International Union of Crystallography by D. Reidel, 1981. 440 p.
142. Ihee H. [et al.] Ultrafast electron diffraction and structural dynamics: transient intermediates in the elimination reaction of $\text{C}_2\text{F}_4\text{I}_2$ // *J. Phys. Chem. A*. 2002. V. 106, № 16. P. 4087–4103.
143. Mironov B.N. [et al.] Direct observation of the generation of coherent optical phonons in thin antimony films by the femtosecond electron diffraction method // *JETP Lett.* 2016. V. 103, № 8. P. 531–534.
144. Ischenko A.A., Schäfer L., Tarasov Yu.I., Ryabov E.A., Aseyev S.A. Ultrafast transmission electron microscopy // *Tonkie khimicheskie tekhnologii (Fine Chem. Technol.)*. 2017. V. 12, № 1. P. 5–25.
145. Schelev M.Y. [et al.] Aspects of streak image tube photography (*Advances in Imaging and Electron Physics*, V. 180). Amsterdam: Academic Press, 2013.
146. Degtyareva V.P. [et al.] Femtosecond streak tubes designing, manufacturing, and testing // *Proc. SPIE 4948, 25th Int. Congress on High-Speed Photography and Photonics*, (1 August 2003) / ed. Cavailler C., Haddleton G.P., Hugenschmidt M. 2003. P. 281.
147. Degtyareva V.P. [et al.] Dynamic parameters evaluation for femtosecond streak tubes // *Proc. SPIE 5580, 26th Int. Congress on High-Speed Photography and Photonics*, (17 March 2005 / ed. Paisley D.L. [et al.] 2005. P. 416.
148. Andreev S.A. [et al.] The results of computer

and experimental studies on compressing the ultrashort photoelectron bunches with time-dependent electric fields // Proc. SPIE 6279, 27th Int. Congress on High-Speed Photography and Photonics January 2007 / ed. Hou X., Zhao W., Yao B. 2007. P. 6279 70.

149. Ageeva N. V. [et al.] Sub-100 fs streak tube: computer-aided design, manufacturing, and testing // Proc. SPIE 7126, 28th Int. Congress on High-Speed Imaging and Photonics, 71261B (10 February 2009) / ed. Kleine H., Butron Guillen M.P. 2009. P. 7126 1B.

150. Degtyareva V.P., Monastyrskiy M.A., Schelev M.Y. Chapter 11 // Electron Diffraction: Structure and Dynamics of Free Molecules and Condensed Matter. Moscow: FIZMATLIT, 2013. P. 499–522 (in Russ.).

151. Hansen P. [et al.] Dispersion compensation for attosecond electron pulses // Appl. Phys. Lett. 2012. V. 101, № 8. P. 83501.

152. Fortov V.E. Extreme states of matter on Earth and in space // Physics-Uspekhi. 2009. V. 52,

№ 6. P. 615–647.

153. Zewail A.H. The new age of structural dynamics // Acta Crystallogr. Sect. A. Found. Crystallogr. 2010. V. 66, № 2. P. 135–136.

154. Zewail A., Zewail M. Science for the “Haves” // Angew. Chemie Int. Ed. 2013. V. 52, № 1. P. 108–111.

155. Alidzhanov E.K. [et al.] Vacuum scanning tunnel microscope for conducting samples researching // Vestnik Orenburg. Gos. Univ. 2007. № 12. P. 150–153 (in Russ.).

156. Aseyev S.A. [et al.] Microscopy of photoionisation processes // Quantum Electron. 2013. V. 43, № 4. P. 308–312.

157. Grams M.P. [et al.] Microscopic fused silica capillary nozzles as supersonic molecular beam sources // J. Phys. D. Appl. Phys. 2006. V. 39, № 5. P. 930–936.

158. Workshop on ultrafast electron sources for diffraction and microscopy applications // UESDM-2012, December 12–14. Univ. of California, Los Angeles, USA, 2012.

About the authors:

Anatoly A. Ischenko, Dr.Sci. (Chemistry), Professor, Head of Alimarin Department of Analytical Chemistry, Institute of Fine Chemical Technologies, Moscow Technological University (86, Vernadskogo pr., Moscow 119571, Russia).

Yury I. Tarasov, Dr.Sci. (Phys.-Mathematics), Professor, Head of Department of Physics and Technical Mechanics, Institute of Fine Chemical Technologies, Moscow Technological University (86, Vernadskogo pr., Moscow 119571, Russia).

Lothar Schäfer, Professor, Department of Chemistry and Biochemistry, University of Arkansas (Fayetteville, AR, U.S.A., AR72701).

Об авторах:

Ищенко Анатолий Александрович, доктор химических наук, профессор, заведующий кафедрой аналитической химии им. И.П. Алимарины Института тонких химических технологий ФГБОУ ВО «Московский технологический университет» (119571, Россия, Москва, пр-т Вернадского, д. 86).

Тарасов Юрий Игоревич, доктор физико-математических наук, профессор, заведующий кафедрой физики и технической механики Института тонких химических технологий ФГБОУ ВО «Московский технологический университет» (119571, Россия, Москва, пр-т Вернадского, д. 86).

Шефер Лотар, профессор, Факультет химии и биохимии, Университет штата Арканзас (Фэйтвилл, 72701, Арканзас, США).